teraction module (Dawid et al., 1998; Bach, 2000). The LIM domains of Zyxin interact with members of CRP family (Sadler et al., 1992) and serine/threonine kinase h-warts/LATS1 (Hirota et al., 2000). During mitosis, phosphorylation of Zyxin by Cdc2 promotes the binding between Zyxin and h-warts/LATS1, and the complex is targeted to the mitotic apparatus. The possibility that interaction between CSX/NKX2-5 and Cal is modulated by specific protein modification remains to be determined.

Abundant expression of *Cal* was detected in the heart during embryogenesis and maintained in the atrial and ventricular chambers through the adulthood. *Cal* was also expressed in a variety of tissues such as the aorta, lung, and intestine, but little expression was detected in the brain and liver. Although the functional roles of Cal in tissues other than the heart remain unknown at present, Cal may associate with other NK homeobox transcription factors, because the amino acid sequences of homeodomains, which are responsible for binding to Cal, are highly conserved among this class of homeoproteins. Interestingly, Ajuba has been reported to associate with thyroid transcription factor-1/Nkx2-1, a member of NK homeobox transcription factors, in mammalian cells, although the physiological function of their interaction remains unknown (Missero et al., 2001). It is possible that there are more combinatorial patterns of physical interaction between Zyxin family LIM proteins and NK homeoproteins.

Cal shuttles between the cytoplasm and the nucleus

The leucine-rich sequence of Cal is thought to function as an NES, based on the following results: (a) the leucine-rich sequence of Cal matches the consensus of the NES; (b) predominant nuclear distribution was observed when treated with LMB, that is a specific inhibitor of CRM1-dependent nuclear export (Kudo et al., 1998); (c) the Cal mutant lacking the leucine-rich sequence was localized predominantly in the nucleus; and (d) fusion of leucine-rich sequence of Cal to Rev1.4-EGFP transported the Rev1.4-EGFP from the nucleus to the cytoplasm (Henderson, 2000). Functional leucine-rich NESs have been identified in other Zyxin family members such as *Zyxin* (Nix and Beckerle, 1997), *trip6* (Wang and Gilmore, 2001), *LPP* (Petit et al., 2000), and *Ajuba* (Kanungo et al., 2000). Although the role of Zyxin family members in the nucleus has not been fully defined, the interaction between Zyxin and h-wartz/LATS1 on the mitotic apparatus implicates the specific role of Zyxin in the regulation of cell cycle (Hirota et al., 2000).

Cal augments CSX/NKX2-5–induced promoter activation

The interaction between CSX/NKX2-5 and Cal implicates a certain role of transcriptional regulation of cardiac-specific genes. CSX/NKX2-5 and Cal synergistically activated both the *ANP* promoter and the artificial promoter containing multimerized CSX/NKX2-5–binding sites. Furthermore, Cal enhanced cooperative promoter activation of *ANP* gene between CSX/NKX2-5 and GATA-4 or Tbx-5. These results suggest that transcriptional regulation by cardiac transcription factors may be fulfilled harmoniously by multiprotein complex.

The GAL4-based reporter assay revealed that Cal itself possesses transcriptional activity. LIM2 and LIM3 domains were endowed with the capacity to activate transcription, whereas the LIM1 domain suppressed the transcriptional activity. On the other hand, the ΔLIM1 mutant failed to augment CSX/NKX2-5–induced transactivation of the *ANP* reporter (Fig. 3 B). GST pull-down assays revealed that the LIM domains are required for binding to CSX/NKX2-5 and that deletion of LIM1 reduced the mutual binding (Fig. 2 C), suggesting that deletion of LIM1 may also decrease the binding affinity for CSX/NKX2-5. In addition, there is a possibility that the LIM1 interferes the GAL4-DNA binding but not inhibits the transcription. It has been reported that Trip6 and LPP have transcriptional activity, and the transactivation domains were attributed to the LIM domains and a region containing the NES of *trip6* (Wang and Gilmore, 2001) and to the LIM domains and the proline-rich region of *LPP* (Kanungo et al., 2000). Based on the fact that transactivation domains reside in modules for protein–protein interaction, it is likely that the interaction with components of transcriptional initiation complex is involved in transcriptional activation.

Cooperative transactivation of the *ANP* promoter by CSX/NKX2-5 and Cal was enhanced when Cal protein was targeted into the nucleus by deleting its NES. We found that treatment with Ca^{2+} ionophore A23187 induced nuclear transport of Cal. Pathophysiological significance of Ca^{2+} signaling in cardiac development has not been fully defined. However, Ca^{2+} signals are induced by various conditions including G-protein–coupled receptors (Clapham, 1995) and receptor tyrosine kinases (Schlessinger, 2000). It is possible to assume that Cal might modulate the transcriptional activity of CSX/NKX2-5 in response to Ca^{2+} signals triggered by G-protein–coupled receptors or receptor tyrosine kinases during cardiogenesis. Exploration of physiological ligands that activate Ca^{2+} signals and subsequent nuclear import of Cal will undermine the molecular framework of cardiac development.

Ca^{2+} signaling plays an important role in generation of cardiac hypertrophy (Frey et al., 2000). Nuclear import of NF-AT transcription factors is induced by Ca^{2+}-activated phosphatase calcineurin and that transgenic mice expressing nuclear form of NF-AT3 in the heart exhibited cardiac hypertrophy (Molkentin et al., 1998). CSX/NKX2-5 is expressed in the adult heart (Komuro and Izumo, 1993), and it has been proposed that CSX/NKX2-5 is involved in generation of cardiac hypertrophy (Akazawa and Komuro, 2003) on the basis of in vivo findings that expression levels of CSX/NKX2-5 were increased in response to hypertrophic stimuli including pressure overload (Thompson et al., 1998) and phenylephrine or isoproterenol (Saadane et al., 1999). Therefore, Cal may be another Ca^{2+}-sensitive effector that translocates into the nucleus like NF-AT transcription factors and it is possible to speculate that Cal may play a certain role in generation of cardiac hypertrophy by modulating transcriptional activity of CSX/NKX2-5.

Cal may function as a signal mediator that links cytoplasmic signals and gene expression

Cal was localized in the cytoplasm at steady state and translocated into the nucleus in response to calcium, and Cal functioned as a transcriptional activator in the nucleus by cooper-

ating with the cardiac transcription factor CSX/NKX2-5. These results indicate a novel function of LIM proteins that link cytoplasmic signals and nuclear gene expression.

Recently, some proteins associated with cell junctions have been reported to be involved in transcriptional regulation. A membrane-associated guanylate kinase, CASK/LIN-2, interacts with a T-box transcription factor, Tbr-1, and stimulates the transcriptional activity of Tbr-1 in the nucleus of mammalian cells (Hsueh et al., 2000). Jun activation domain-binding protein 1, colocalizing with integrin LFA-1, translocates into the nucleus in response to LFA-1 stimulation and acts as a coactivator for AP-1 complex (Bianchi et al., 2000). β-Catenin, linking cadherins to actin cytoskeleton at adherens junctions, interacts with T cell factor to form a transcriptional activator complex in response to Wnt signaling (Barth et al., 1997). Although CRP3/MLP binds to Zyxin and α actinin in the cytoplasm (Louis et al., 1997), forced expression of CRP3/MLP in the nucleus by fusing it to nuclear localization signal led to a cooperative enhancement of the transcriptional activity of MyoD (Kong et al., 1997). Trip6 also acts as a coactivator for v-Rel transcription factor (Zhao et al., 1999). However, it remains unclear how subcellular localization of CRP3/MLP and trip6 is regulated. We first clarify the molecular mechanism of how the cytoplasmic LIM protein is translocated into the nucleus and functions as a transcriptional activator.

Cal promotes cardiac differentiation in P19CL6 cells

Mouse P19CL6 cells, derived from P19 embryonal carcinoma cells, are used as a good in vitro system for molecular analysis of cardiac differentiation. In the presence of 1% DMSO, mouse P19CL6 cell efficiently differentiate into spontaneously beating cardiac myocytes that exhibit the biological features recapturing embryonic cardiogenesis in vivo (Monzen et al., 1999, 2001). P19CL6 cells that overexpress nuclear form of Cal (P19CL6-Cal-ΔNES) differentiated into cardiac myocytes more efficiently than the parental P19CL6 cells. In P19CL6-Cal-ΔNES cells, expression levels of *SERCA2*, *calreticulin*, *connexin43*, *ANP*, and *cardiac troponin T* were up-regulated, which convey properties characteristic of cardiomyocytes. Expression levels of cardiac transcription factor *MEF2C* did not change, whereas expression levels of *GATA-4* were increased. Although there has been no evidence indicating that *GATA-4* is a downstream target for CSX/NKX2-5, it is possible that expression of *GATA-4* is up-regulated through undefined functions of Cal. Up-regulation of *GATA-4* might have an influence on myocardial cell differentiation in P19CL6-Cal-ΔNES. These results leave an open question whether the nuclear target for Cal is solely CSX/NKX2-5. However, based on the up-regulated expression of the target genes for CSX/NKX2-5, it is reasonable to assume that cooperation of CSX/NKX2-5 and Cal promoted cardiac differentiation in P19CL6 cells. Our present studies elucidate a novel role of LIM proteins in cardiac development as a transcriptional activator, and suggest that fine-tuned gene expression during cardiogenesis is orchestrated by multiprotein complex including LIM proteins as well as transcription factors.

Materials and methods

Molecular cloning of Cal

We performed a yeast two-hybrid screening using the MATCHMAKER Two-Hybrid System (CLONTECH Laboratories, Inc.) as described previously (Hiroi et al., 2001). The plasmid pGBT9-CSX, which encodes the GAL4 DNA-binding domain fused to the human CSX/NKX2-5, was used as a bait in screening of a human heart MATCHMAKER cDNA Library (CLONTECH Laboratories, Inc.). One clone containing a fragment of CAL cDNA was scored positive, and the full-length mouse Cal cDNA was obtained by screening a mouse heart cDNA library (Stratagene).

Northern blot, RT-PCR, and in situ hybridization analysis

For Northern blot analysis, total RNA was hybridized with cDNA corresponding to 3'-UTR of *Cal*. Probes for *GATA-4*, *MEF2C*, *connexin 43*, and *SERCA2* were described previously (Hiroi et al., 2001). A probe for *calreticulin* was a gift from M. Michalak (University of Alberta, Alberta, Canada). RT-PCR analysis for *ANP* expression was performed as described previously (Hiroi et al., 2001). Digoxygenin labeled riboprobes were synthesized by using the 1.5-kb *Cal* cDNA, and RNA in situ hybridization was performed as described previously (Akazawa et al., 2000).

Plasmids construction

The following plasmids were described previously: the expression vectors of CSX/NKX2-5 (pEFSA-HA-CSX), GATA-4 (pSSRa-hGATA4), and Tbx-5 (pcDNA3-Tbx5); the luciferase reporters containing the *ANP* promoter (ANP[600]-Luc and ANP[2600]-Luc); and multimerized CSX-binding sites (4×TTF-Luc; Shiojima et al., 1999; Hiroi et al., 2001). FLAG-tagged Cal was subcloned into pCAGGS vector (pCAGGS-FLAG-Cal; Niwa et al., 1991; Aoki et al., 2000). pCAGGS vector was provided by J. Miyazaki (Osaka University Graduate School of Medicine, Suita, Japan) and T. Kobayashi and O. Hino (The Cancer Institute, Japanese Foundation for Cancer Research, Tokyo, Japan). Cal derivatives were subcloned into pcDNA3.1 (Invitrogen) and pBIND (Promega) for in vitro transcription and translation and expression of GAL4-fusion protein, respectively. For deletion analyses, the following Cal derivatives were subcloned into the corresponding vectors: Cal-ΔLIM1 (1-184, 221-375), Cal-ΔLIM2 (1-244, 279-375), Cal-ΔLIM3 (1-307, 345-375), Cal-ΔLIM123 (1-184), Cal-LIM123 (185-375), Cal-LIM23 (245-375), and Cal-ΔNES (1-121, 135-375).

Cell culture, transfection, and reporter gene assay

Primary cultures of cardiac myocytes were prepared from ventricles of 1-d-old Wistar rats as described previously (Kudoh et al., 1997). Transient transfections were performed by standard calcium phosphate methods. For reporter gene assays, pRL-SV40 (Promega) was cotransfected as an internal control. Luciferase activities were measured as described previously (Shiojima et al., 1999). P19CL6 cells were cultured as described previously (Monzen et al., 1999). To isolate the permanent cell lines, P19CL6 cells were transfected with pcDNA3.1-Cal and pcDNA3.1-Cal-ΔNES by the lipofection method (TfxTM reagents; Promega). Stable transformants were selected with 400 μg/ml of neomycin (G418; Sigma-Aldrich).

Coimmunoprecipitation experiment

We performed a coimmunoprecipitation experiment as described previously (Shiojima et al., 1999). COS-7 cells were transiently transfected with expression plasmids of pEFSA-HA-CSX and pCAGGS-FLAG-Cal or pCAGGS-FLAG-CalΔNES. For preparation of the cytoplasmic fraction, transfected cells were lysed in digitonin buffer (20 mM Hepes/KOH, pH 7.5, 150 mM NaCl, 1 mM EDTA, and 50 μg/ml digitonin) on ice for 10 min. The lysates were centrifuged at 1,000 *g* and the supernatant was collected as the cytoplasmic fraction. The pellets were resuspended Triton buffer (20 mM Hepes/KOH, pH 7.5, 150 mM NaCl, 1 mM EDTA, and 10 mg/ml Triton X-100) and the lysates were used as the nuclear fraction. Protein samples were subjected to immunoprecipitation with the anti-FLAG mAb M2 (KODAK), fractionated by 10% SDS-PAGE, and immunoblotted with the rabbit polyclonal anti-HA antibody (Santa Cruz Biotechnology, Inc.). HRP-conjugated anti-rabbit IgG antibody was used as the secondary antibody and immune complex was detected by the ECL detection kit (Amersham Biosciences).

GST pull-down assay

We performed GST pull-down assays as described previously (Shiojima et al., 1999). GST fusion protein of CSX/NKX2-5 has been described previously. cDNA fragment corresponding to the full length of Cal was subcloned in frame into the EcoRI site of pGEX-3X (Amersham Biosciences). CSX/NKX2-5 derivatives (Shiojima et al., 1999) and Cal derivatives, subcloned

into pcDNA3.1 vector (Invitrogen), were labeled with [^{35}S]methionine by the TNT Quick Coupled Transcription/Translation Systems (Promega). GST and GST fusion proteins immobilized on glutathione-Sepharose 4B beads were mixed with in vitro–translated proteins. Bound proteins were fractionated by SDS-PAGE and visualized by autoradiography.

Immunostaining

Rat neonatal cardiac myocytes or HeLa cells were transfected with the expression vector of Cal and Cal mutants. Cells were stained with the anti-FLAG mAb M2 (KODAK), and visualized with FITC-labeled anti–mouse IgG (CAPPEL). Calcium ionophore A23187 was purchased from Sigma-Aldrich. Differentiated P19CL6 cells were stained with anticardiac troponin T mAb (Deutsche Sammlung von Mikroorganismen und Zellkulturen GmbH) and visualized with Cy3-labeled anti–mouse IgG (CHEMICON International, Inc.). The cells were double stained using rhodamine-phalloidin (Molecular Probes) or TO-PRO-3 (Molecular Probes).

Nuclear export assays

Nuclear export assays were performed as described previously (Henderson, 2000). pRev(1.4)-NES-EGFP plasmid was constructed by subcloning the NES of Cal between BamHI and AgeI sites of pRev(1.4)-EGFP plasmid (provided by B.R. Henderson, Westmead Institute for Cancer Research, Sydney, Australia). The NES of Cal was amplified by PCR using specific primers (5′-AGGGAAGCCCCCACCCCCGCCTC-3′, and 5′-GGTGGGGGCTTCCCTG-GTAAGACA-3′). Actinomycin D (Sigma-Aldrich) was added at 5 mg/ml to prevent nucleolar association of Rev protein. LMB was provided by M. Yoshida (The University of Tokyo, Tokyo, Japan).

Acquisition and processing of images

For light microscopic analysis (Fig. 1 C), images were acquired by a stereomicroscope (MZ12; objective lens, Plan 1.0×; Leica) and captured by DC100 program (Leica), or by a light microscope (Axioskop 2 plus; objective lens, Plan-Neofluar 2.5×/0.075; Carl Zeiss MicroImaging, Inc.) and captured by Axio Cam CCD camera and Axio Vision 3.0 imaging system (Carl Zeiss MicroImaging, Inc.). For immunofluorescence microscopic analysis, images were acquired by a laser-scanning microscope (model Eclipse E600; Nikon) using Plan-Fluor 10×/0.30 (Fig. 7 B), Plan-Fluor 40×/0.75 (Fig. 6 A), and Plan-Apo 60×A/1.40 oil (Fig. 5). Radiance 2000 confocal scanning system (Bio-Rad Laboratories) was used.

Accession no.

The deduced amino acid sequence of mouse Cal was deposited in GenBank/EMBL/DDBJ accession no. AF513359.

We thank Ms. R. Kobayashi, E. Fujita, and M. Watanabe for their excellent technical assistance.

This work was supported in part by grants from the Japanese Ministry of Education, Science, Sports, and Culture, and Japan Health Sciences Foundation (JHSF; to I. Komuro), Japanese Heart Foundation and Kanae Foundation for Life and Sociomedical Science (to H. Akazawa). H. Akazawa is a Research Resident for Research on Human Genome, Tissue Engineering Food Biotechnology of JHSF.

Submitted: 26 September 2003
Accepted: 29 December 2003

References

Akazawa, H., and I. Komuro. 2003. Roles of cardiac transcription factors in cardiac hypertrophy. *Circ. Res.* 92:1079–1088.

Akazawa, H., I. Komuro, Y. Sugitani, Y. Yazaki, R. Nagai, and T. Noda. 2000. Targeted disruption of the homeobox transcription factor Bapx1 results in lethal skeletal dysplasia with asplenia and gastroduodenal malformation. *Genes Cells.* 5:499–513.

Aoki, H., J. Hayashi, M. Moriyama, Y. Arakawa, and O. Hino. 2000. Hepatitis C virus core protein interacts with 14-3-3 protein and activates the kinase Raf-1. *J. Virol.* 74:1736–1741.

Arber, S., and P. Caroni. 1996. Specificity of single LIM motifs in targeting and LIM/LIM interactions in situ. *Genes Dev.* 10:289–300.

Arber, S., G. Halder, and P. Caroni. 1994. Muscle LIM protein, a novel essential regulator of myogenesis, promotes myogenic differentiation. *Cell.* 79: 221–231.

Arber, S., J.J. Hunter, J. Ross, Jr., M. Hongo, G. Sansig, J. Borg, J.C. Perriard, K.R. Chien, and P. Caroni. 1997. MLP-deficient mice exhibit a disruption of cardiac cytoarchitectural organization, dilated cardiomyopathy, and heart failure. *Cell.* 88:393–403.

Bach, I. 2000. The LIM domain: regulation by association. *Mech. Dev.* 91:5–17.

Barth, A.I., I.S. Nathke, and W.J. Nelson. 1997. Cadherins, catenins and APC protein: interplay between cytoskeletal complexes and signaling pathways. *Curr. Opin. Cell Biol.* 9:683–690.

Beckerle, M.C. 1997. Zyxin: zinc fingers at sites of cell adhesion. *Bioessays.* 19: 949–957.

Bianchi, E., S. Denti, A. Granata, G. Bossi, J. Geginat, A. Villa, L. Rogge, and R. Pardi. 2000. Integrin LFA-1 interacts with the transcriptional co-activator JAB1 to modulate AP-1 activity. *Nature.* 404:617–621.

Bruneau, B.G., G. Nemer, J.P. Schmitt, F. Charron, L. Robitaille, S. Caron, D.A. Conner, M. Gessler, M. Nemer, C.E. Seidman, and J.G. Seidman. 2001. A murine model of Holt-Oram syndrome defines roles of the T-box transcription factor Tbx5 in cardiogenesis and disease. *Cell.* 106:709–721.

Chen, C.Y., and R.J. Schwartz. 1996. Recruitment of the tinman homolog Nkx-2.5 by serum response factor activates cardiac alpha-actin gene transcription. *Mol. Cell. Biol.* 16:6372–6384.

Clapham, D.E. 1995. Calcium signaling. *Cell.* 80:259–268.

Dawid, I.B., J.J. Breen, and R. Toyama. 1998. LIM domains: multiple roles as adapters and functional modifiers in protein interactions. *Trends Genet.* 14: 156–162.

Durocher, D., F. Charron, R. Warren, R.J. Schwartz, and M. Nemer. 1997. The cardiac transcription factors Nkx2-5 and GATA-4 are mutual cofactors. *EMBO J.* 16:5687–5696.

Fornerod, M., M. Ohno, M. Yoshida, and I.W. Mattaj. 1997. CRM1 is an export receptor for leucine-rich nuclear export signals. *Cell.* 90:1051–1060.

Frey, N., T.A. McKinsey, and E.N. Olson. 2000. Decoding calcium signals involved in cardiac growth and function. *Nat. Med.* 6:1221–1227.

Gertler, F.B., K. Niebuhr, M. Reinhard, J. Wehland, and P. Soriano. 1996. Mena, a relative of VASP and *Drosophila* Enabled, is implicated in the control of microfilament dynamics. *Cell.* 87:227–239.

Goyal, R.K., P. Lin, J. Kanungo, A.S. Payne, A.J. Muslin, and G.D. Longmore. 1999. Ajuba, a novel LIM protein, interacts with Grb2, augments mitogen-activated protein kinase activity in fibroblasts, and promotes meiotic maturation of *Xenopus* oocytes in a Grb2- and Ras-dependent manner. *Mol. Cell. Biol.* 19:4379–4389.

Henderson, B.R. 2000. Nuclear-cytoplasmic shuttling of APC regulates beta-catenin subcellular localization and turnover. *Nat. Cell Biol.* 2:653–660.

Hiroi, Y., S. Kudoh, K. Monzen, Y. Ikeda, Y. Yazaki, R. Nagai, and I. Komuro. 2001. Tbx5 associates with Nkx2-5 and synergistically promotes cardiomyocyte differentiation. *Nat. Genet.* 28:276–280.

Hirota, T., T. Morisaki, Y. Nishiyama, T. Marumoto, K. Tada, T. Hara, N. Masuko, M. Inagaki, K. Hatakeyama, and H. Saya. 2000. Zyxin, a regulator of actin filament assembly, targets the mitotic apparatus by interacting with h-warts/LATS1 tumor suppressor. *J. Cell Biol.* 149:1073–1086.

Hobert, O., J.W. Schilling, M.C. Beckerle, A. Ullrich, and B. Jallal. 1996. SH3 domain-dependent interaction of the proto-oncogene product Vav with the focal contact protein zyxin. *Oncogene.* 12:1577–1581.

Hsueh, Y.P., T.F. Wang, F.C. Yang, and M. Sheng. 2000. Nuclear translocation and transcription regulation by the membrane-associated guanylate kinase CASK/LIN-2. *Nature.* 404:298–302.

Kanungo, J., S.J. Pratt, H. Marie, and G.D. Longmore. 2000. Ajuba, a cytosolic LIM protein, shuttles into the nucleus and affects embryonal cell proliferation and fate decisions. *Mol. Biol. Cell.* 11:3299–3313.

Komuro, I., and S. Izumo. 1993. Csx: a murine homeobox-containing gene specifically expressed in the developing heart. *Proc. Natl. Acad. Sci. USA.* 90: 8145–8149.

Kong, Y., M.J. Flick, A.J. Kudla, and S.F. Konieczny. 1997. Muscle LIM protein promotes myogenesis by enhancing the activity of MyoD. *Mol. Cell. Biol.* 17:4750–4760.

Kudo, N., B. Wolff, T. Sekimoto, E.P. Schreiner, Y. Yoneda, M. Yanagida, S. Horinouchi, and M. Yoshida. 1998. Leptomycin B inhibition of signal-mediated nuclear export by direct binding to CRM1. *Exp. Cell Res.* 242:540–547.

Kudoh, S., I. Komuro, T. Mizuno, T. Yamazaki, Y. Zou, I. Shiojima, N. Takekoshi, and Y. Yazaki. 1997. Angiotensin II stimulates c-Jun NH2-terminal kinase in cultured cardiac myocytes of neonatal rats. *Circ. Res.* 80:139–146.

Kuersten, S., M. Ohno, and I.W. Mattaj. 2001. Nucleocytoplasmic transport: Ran, beta and beyond. *Trends Cell Biol.* 11:497–503.

Lee, Y., T. Shioi, H. Kasahara, S.M. Jobe, R.J. Wiese, B.E. Markham, and S. Izumo. 1998. The cardiac tissue-restricted homeobox protein Csx/Nkx2.5 physically associates with the zinc finger protein GATA4 and cooperatively activates atrial natriuretic factor gene expression. *Mol. Cell. Biol.* 18:3120–3129.

Lints, T.J., L.M. Parsons, L. Hartley, I. Lyons, and R.P. Harvey. 1993. Nkx-2.5: a novel murine homeobox gene expressed in early heart progenitor cells and their myogenic descendants. *Development.* 119:969.

Louis, H.A., J.D. Pino, K.L. Schmeichel, P. Pomies, and M.C. Beckerle. 1997. Comparison of three members of the cysteine-rich protein family reveals functional conservation and divergent patterns of gene expression. *J. Biol. Chem.* 272:27484–27491.

Lyons, I., L.M. Parsons, L. Hartley, R. Li, J.E. Andrews, L. Robb, and R.P. Harvey. 1995. Myogenic and morphogenetic defects in the heart tubes of murine embryos lacking the homeo box gene Nkx2-5. *Genes Dev.* 9:1654–1666.

Mahoney, N.M., P.A. Janmey, and S.C. Almo. 1997. Structure of the profilin-poly-L-proline complex involved in morphogenesis and cytoskeletal regulation. *Nat. Struct. Biol.* 4:953–960.

Mattaj, I.W., and L. Englmeier. 1998. Nucleocytoplasmic transport: the soluble phase. *Annu. Rev. Biochem.* 67:265–306.

Missero, C., M.T. Pirro, S. Simeone, M. Pischetola, and R. Di Lauro. 2001. The DNA glycosylase T:G mismatch-specific thymine DNA glycosylase represses thyroid transcription factor-1-activated transcription. *J. Biol. Chem.* 276: 33569–33575.

Molkentin, J.D., J.R. Lu, C.L. Antos, B. Markham, J. Richardson, J. Robbins, S.R. Grant, and E.N. Olson. 1998. A calcineurin-dependent transcriptional pathway for cardiac hypertrophy. *Cell.* 93:215–228.

Monzen, K., I. Shiojima, Y. Hiroi, S. Kudoh, T. Oka, E. Takimoto, D. Hayashi, T. Hosoda, A. Habara-Ohkubo, T. Nakaoka, et al. 1999. Bone morphogenetic proteins induce cardiomyocyte differentiation through the mitogen-activated protein kinase kinase kinase TAK1 and cardiac transcription factors Csx/Nkx-2.5 and GATA-4. *Mol. Cell. Biol.* 19:7096–7105.

Monzen, K., Y. Hiroi, S. Kudoh, H. Akazawa, T. Oka, E. Takimoto, D. Hayashi, T. Hosoda, M. Kawabata, K. Miyazono, et al. 2001. Smads, TAK1, and their common target ATF-2 play a critical role in cardiomyocyte differentiation. *J. Cell Biol.* 153:687–698.

Niwa, H., K. Yamamura, and J. Miyazaki. 1991. Efficient selection for high-expression transfectants with a novel eukaryotic vector. *Gene.* 108:193–199.

Nix, D.A., and M.C. Beckerle. 1997. Nuclear-cytoplasmic shuttling of the focal contact protein, zyxin: a potential mechanism for communication between sites of cell adhesion and the nucleus. *J. Cell Biol.* 138:1139–1147.

Ohno, M., M. Fornerod, and I.W. Mattaj. 1998. Nucleocytoplasmic transport: the last 200 nanometers. *Cell.* 92:327–336.

Petit, M.M., R. Mols, E.F. Schoenmakers, N. Mandahl, and W.J. Van de Ven. 1996. LPP, the preferred fusion partner gene of HMGIC in lipomas, is a novel member of the LIM protein gene family. *Genomics.* 36:118–129.

Petit, M.M., J. Fradelizi, R.M. Golsteyn, T.A. Ayoubi, B. Menichi, D. Louvard, W.J. Van de Ven, and E. Friederich. 2000. LPP, an actin cytoskeleton protein related to zyxin, harbors a nuclear export signal and transcriptional activation capacity. *Mol. Biol. Cell.* 11:117–129.

Prehoda, K.E., D.J. Lee, and W.A. Lim. 1999. Structure of the enabled/VASP homology 1 domain-peptide complex: a key component in the spatial control of actin assembly. *Cell.* 97:471–480.

Renfranz, P.J., and M.C. Beckerle. 2002. Doing (F/L)PPPPs: EVH1 domains and their proline-rich partners in cell polarity and migration. *Curr. Opin. Cell Biol.* 14:88–103.

Saadane, N., L. Alpert, and L.E. Chalifour. 1999. Expression of immediate early genes, GATA-4, and Nkx-2.5 in adrenergic-induced cardiac hypertrophy and during regression in adult mice. *Br. J. Pharmacol.* 127:1165–1176.

Sadler, I., A.W. Crawford, J.W. Michelsen, and M.C. Beckerle. 1992. Zyxin and cCRP: two interactive LIM domain proteins associated with the cytoskeleton. *J. Cell Biol.* 119:1573–1587.

Schlessinger, J. 2000. Cell signaling by receptor tyrosine kinases. *Cell.* 103:211–225.

Schott, J.J., D.W. Benson, C.T. Basson, W. Pease, G.M. Silberbach, J.P. Moak, B.J. Maron, C.E. Seidman, and J.G. Seidman. 1998. Congenital heart disease caused by mutations in the transcription factor NKX2-5. *Science.* 281: 108–111.

Shiojima, I., I. Komuro, T. Oka, Y. Hiroi, T. Mizuno, E. Takimoto, K. Monzen, R. Aikawa, H. Akazawa, T. Yamazaki, et al. 1999. Context-dependent transcriptional cooperation mediated by cardiac transcription factors Csx/Nkx-2.5 and GATA-4. *J. Biol. Chem.* 274:8231–8239.

Thompson, J.T., M.S. Rackley, and T.X. O'Brien. 1998. Upregulation of the cardiac homeobox gene Nkx2-5 (CSX) in feline right ventricular pressure overload. *Am. J. Physiol.* 274:H1569–H1573.

Wang, Y., and T.D. Gilmore. 2001. LIM domain protein Trip6 has a conserved nuclear export signal, nuclear targeting sequences, and multiple transactivation domains. *Biochim. Biophys. Acta.* 1538:260–272.

Yi, J., and M.C. Beckerle. 1998. The human TRIP6 gene encodes a LIM domain protein and maps to chromosome 7q22, a region associated with tumorigenesis. *Genomics.* 49:314–316.

Zhao, M.K., Y. Wang, K. Murphy, J. Yi, M.C. Beckerle, and T.D. Gilmore. 1999. LIM domain-containing protein trip6 can act as a coactivator for the v-Rel transcription factor. *Gene Expr.* 8:207–217.

Cellular/Molecular

A Truncated Tropo-Myosine-Related Kinase B Receptor, T1, Regulates Glial Cell Morphology via Rho GDP Dissociation Inhibitor 1

Koji Ohira,[1,2] Haruko Kumanogoh,[1] Yoshinori Sahara,[1] Koichi J. Homma,[3] Hirohisa Hirai,[2] Shun Nakamura,[1] and Motoharu Hayashi[2]

[1]Department of Biochemistry and Cellular Biology, National Institute of Neuroscience, National Center of Neurology and Psychiatry, Tokyo 187-8502, Japan, [2]Department of Cellular and Molecular Biology, Primate Research Institute, Kyoto University, Inuyama, Aichi 484-8506, Japan, and [3]Department of Molecular Pathology, Faculty of Pharmaceutical Sciences, Teikyo University, Kanagawa 199-0195, Japan

Through tropo-myosine-related kinase B (TrkB) receptors, brain-derived neurotrophic factor (BDNF) performs many biological functions such as neural survival, differentiation, and plasticity. T1, an isoform of TrkB receptors that lacks a tyrosine kinase, predominates in the adult mammalian CNS, yet its role remains controversial. In this study, to examine whether T1 transduces a signal and to determine its function, we first performed an affinity purification of T1-binding protein with the T1-specific C-terminal peptide and identified Rho GDP dissociation inhibitor 1 (GDI1), a GDP dissociation inhibitor of Rho small G-proteins, as a signaling protein directly associated with T1. The binding of BDNF to T1 caused Rho GDI1 to dissociate from the C-terminal tail of T1. Astrocytes cultured for 30 d expressed only endogenous T1 among the BDNF receptors. In 30 d cultured astrocytes, Rho GDI1, when dissociated in a BDNF-dependent manner, controlled the activities of the Rho GTPases, which resulted in rapid changes in astrocytic morphology. Furthermore, using 2 d cultured astrocytes that were transfected with T1, a T1 deletion mutant, or cyan fluorescent protein fusion protein of the T1-specific C-terminal sequence, we demonstrated that T1-Rho GDI1 signaling was indispensable for regulating the activities of Rho GTPases and for the subsequent morphological changes among astrocytes. Therefore, these findings indicate that the T1 signaling cascade can alter astrocytic morphology via regulation of Rho GTPase activity.

Key words: astrocyte; BDNF; primary culture; Rho GDI; Rho GTPase; truncated TrkB; T1

Introduction

Brain-derived neurotrophic factor (BDNF) is enriched in the CNS and plays pivotal roles in neural survival, differentiation, and plasticity (Bibel and Barde, 2000; Thoenen, 2000). The effects of BDNF are transduced through the tropo-myosine-related kinase B (TrkB) receptor (Barbacid, 1994). There are three TrkB receptor isoforms in the mammalian CNS (Barbacid, 1994). The full-length isoform (TK+) is a typical tyrosine kinase receptor and transduces the BDNF signal (Kaplan and Miller, 2000). In contrast, two truncated isoforms (TK−: T1 and T2) possess the same extracellular domain, transmembrane domain, and first 12 intracellular amino acid sequences as TK+. However, the C-terminal sequences are the isoform specific (11 and 9 amino acids, respectively) (Barbacid, 1994).

Currently, TK−, especially T1, is hypothesized to be a dominant-negative form of TK+ and is involved in negative functions against TK+, such as the TK+ phosphorylation (Knüsel et al., 1994), the calcium efflux (Eide et al., 1996), the cell survival activity (Haapasalo et al., 2001), and gene expression by BDNF (Offenhäuser et al., 2002). According to this hypothesis, TK− is postulated to form the homodimer or heterodimer with TK+, which prohibits TK+ signaling or limits the availability of BDNF to the neural tissue by trapping excess BDNF.

In contrast, there are several findings that provide evidence against the hypothesis that T1 is a dominant-negative form of TK+. For example, the expression of T1 increases markedly at various important periods in the developing mammalian CNS, such as axonal remodeling and synaptogenesis (Allendoerfer et al., 1994; Fryer et al., 1996; Ohira et al., 1999, 2001). The specific alignment of the intracellular domain of T1 is completely identical among mice, rats, and humans (Klein et al., 1990; Middlemas et al., 1991; Shelton et al., 1995), suggesting that the alignment plays a unique role. In addition, T1 is capable of binding BDNF at the same level as does TK+ (Biffo et al., 1995). As regards the physiological function of T1, it is involved in the control of the elongation of distal dendrites of cortical pyramidal neurons (Ya-

Received May 26, 2004; revised Dec. 20, 2004; accepted Dec. 22, 2004.

This work was supported by Grants-in-Aid for Scientific Research on Priority Areas and the Advanced Brain Science Project (15016056 and 16015341 to M.H. and S.N.); by a Grant-in Aid for the Biodiversity Research of 21st Century Center of Excellence (A14) from the Ministry of Education, Culture, Sports, Science and Technology of Japan; and by Health Sciences Research grants from the Organization of Pharmaceutical Safety and Research and Research on Advanced Medical Technology (nano-1 and MF-3). We thank Dr. Hans Thoenen for his critical reading of this manuscript; Drs. Yoshihiro Sokawa, Shohei Maekawa, Takayoshi Inoue, and Nobuo Funatsu for their helpful comments; and Tomomi Ochiai-Ohira for her photographic expertise.

Correspondence should be addressed to Dr. Motoharu Hayashi, Department of Cellular and Molecular Biology, Primate Research Institute, Kyoto University, Kanrin, Inuyama, Aichi 484-8506, Japan. E-mail: hayashi@pri.kyoto-u.ac.jp.

DOI:10.1523/JNEUROSCI.4436-04.2005

 0270-6474/05/251343-11$15.00/0

coubian and Lo, 2000) and the BDNF-induced calcium entry in astrocytes (Rose et al., 2003). Based on these results, we considered a new hypothesis, namely, that T1 binds to proteins through its C-terminal-specific sequence, which elicits a unique type of signal transduction other than the well understood regulation of the tyrosine kinase pathway. In fact, T1 has been reported to mediate signal transduction (i.e., the acid metabolite release from cells) (Baxter et al., 1997).

To clarify the T1 signaling cascade, in this study, we first performed affinity purification with a T1-specific sequence and then identified Rho GDP dissociation inhibitor 1 (GDI1) as a T1 binding protein from the rat brain. Rho GDI1 is an inhibitory regulator of Rho GTPases that can regulate cell morphology via the remodeling of the cytoskeleton. Furthermore, we provide evidence that T1 is capable of ligand-mediated signaling through Rho GDI1 and of regulating astrocytic morphology in primary cultures.

Materials and Methods

Affinity chromatography. All experimental procedures for animals were performed in accordance with our institutional guidelines (1996). Young adult (4-week-old) Wistar rat whole brains (10 g) were homogenized in 10 vol of homogenization buffer (0.32 M sucrose, 5 mM Tris-HCl, pH 7.5, and 150 mM NaCl containing 1 mM PMSF, 10 μg/ml leupeptine, and 20 μg/ml aprotinin). After centrifugation at 100,000 × *g* at 4°C for 1 h, the supernatant was adjusted to a concentration of 1 mg/ml protein, and this solution was defined as the cytosolic fraction. Eleven synthesized amino acid residues (FVLFHKIPLDG) of the C terminal of T1 were conjugated to a poly-β-hydroxybutyrate-Tenta Gel S (Shimadzu, Kyoto, Japan) matrix. The affinity column was equilibrated with the homogenization buffer. Another column, without the synthetic peptides, was prepared as a control column. Ten milliliter aliquots of the cytosolic fraction were applied to the control column and then were loaded onto the affinity column. After the affinity column was washed with homogenization buffer containing 500 mM NaCl, the bound proteins were eluted in one step with 50 mM glycine, pH 2.5. Ten microliters of each fraction (200 μl) were subjected to SDS-PAGE (10% gel). The proteins in the gels were then silver stained.

Amino acid sequence analysis. The fractions containing the 28 kDa protein, which had been obtained from 20 independent affinity chromatography experiments, were concentrated using Centricon YM-10 (Millipore, Bedford, MA). The proteins were transferred to a polyvinylidene difluoride (PVDF) membrane (Millipore) using a buffer containing 10 mM 3-[(3-cholamidopropyl)dimethylammonio]-1-propanesulfonate and 10% methanol, pH 11. The membranes were stained with 0.1% Ponceau S in 1% acetic acid and were destained with distilled water. For the peptide sequence, immobilized protein bands were cut with 2 mg of CNBr and placed in 200 μl of 70% formic acid in an Eppendorf (Eppendorf Scientific, Westbury, NY) tube overnight. The resulting solution and membranes were dried and then boiled in SDS sample buffer. Tricine-SDS-PAGE was used to segregate the small peptides (<10 kDa) (Ploug et al., 1989). The cut peptides were transferred to PVDF^{SQ} membranes (Millipore), which were then stained with 0.1% Ponceau S in 1% acetic acid and destained with distilled water. The bands were applied to a Sequencer (476A protein sequencer; Applied Biosystems, Foster City, CA).

Cell cultures. For the cell cultures, human embryonic kidney 293 (HEK293) cells were kept in DMEM supplemented with 10% FBS. Astrocytic primary cultures were prepared from neonatal rat pups (Sprague Dawley). The hippocampi were cut into 1 mm slices, incubated in activated papain (20 U/ml, 20 min), and dissociated by gentle trituration (Sahara and Westbrook, 1993). Dissociated astrocytes from neonatal rats were plated at 300,000 cells per dish on cover glasses coated with poly-L-lysine (Sigma, St. Louis, MO). The culture medium contained MEM (Invitrogen, Carlsbad, CA), 0.6% glucose, 5% heat-inactivated FBS, and penicillin–streptomycin (Invitrogen). At 3 d *in vitro* (DIV) after plating, the expression plasmid vectors (see below) were transfected into astrocytes with Lipofectamine 2000 (Invitrogen). At 4 h after transfection, the culture media were exchanged to DMEM containing N2 supplement (Invitrogen). After 24 h, the cells were used for the experiments. For the long-term cultured astrocytes, cells were incubated in DMEM with 5% FBS, and the medium was exchanged every 3 d. At 72 h before the experiments, the culture media were replaced with DMEM containing the N2 supplement. Additionally, the media of all cultures were exchanged for fresh media at 2 h before the experiments.

Reverse-transcription PCR. Total RNA was isolated from primary astrocytes with Isogen (Nippon Gene, Tokyo, Japan). Total RNA (2 μg) was reverse transcribed into cDNA in 20 μl of 1× first-strand buffer containing 0.5 μg of oligo-dT as a primer, 500 μM dNTP, and 200 U of SuperScript II (Invitrogen). PCR was performed in 20 μl of 1× PCR buffer containing 2 μl of reverse transcription (RT) products, 1 U of AmpliTaq DNA polymerase (Roche Applied Science, Basel, Switzerland), 200 μM dNTP, and 0.4 μM of the primer pair. We used the endogenous internal standard (β-actin, 5′-TAAAACGCAGCTCAGTAACAGTCCG-3′ and 5′-TGGAATCCTGTGGCATCCATGAAAC-3′; 348 bp) and specific primers for TK+ (5′-ATAACGGAGACTACACCCTGATGG-3′ and 5′-AGCTGACTGTTGGTGATGCC-3′; 505 bp), T1 (5′-CATAAGATCCCACTGGATGGGTAG-3′ and 5′-GCTGCAGACATCCTCGGAGATTAC-3′; 177 bp), T2 (5′-CAGAAGTGTGCTTATTTTGC-3′ and 5′-AGACAATACAGGTCTACCTCTCAG-3′; 553 bp), or p75 (5′-TGTGTGAAGAGTGCCCAGAG-3′ and 5′-TCACCATATCCGCCACTGTA-3′; 263 bp). The PCR parameters were 94°C for 30 s, 58°C for 30 s, and 72°C for 60 s for 30 cycles, followed by a final elongation at 72°C for 5 min. The amplified PCR products were separated on 1.5% agarose gel.

DNA constructs and transfection. The T1 cDNA obtained from the adult rat cortex was subcloned into the *Eco*RI sites of p internal ribosomal entry site (IRES) 2-enhanced green fluorescent protein (EGFP) (Clontech, Palo Alto, CA), and the resulting construct was designated as pT1-IRES-EGFP. Mutant constructs of T1 were prepared by a PCR mutagenesis method. Briefly, we used the 5′ primer for T1, GGTCTGCCGTCTGCACGTCTG, and the 3′ primers A, CGCGGATCCCTAGAGCAGAAGCAGCATC; B, CGCGGATCCTTAACCTTTCATGCC; C, CGCGGATCCCTAAACAAAACCTTTC; D, CGCGGATCCCTAATGAAACAAAACAAAAC; and E, CGCGGATCCCTAGGGGATCTTATG. The underlined sequences indicate the *Bam*H1 sites. The boldface letters represent mutation sites. PCR was performed at 94°C for 30 s, 58°C for 30 s, and 72°C for 60 s for 30 cycles, followed by a final elongation at 72°C for 5 min with an Expand High Fidelity PCR system (Roche Applied Science). The amplified PCR products were separated on 2% agarose gel. The PCR products were digested at the 5′ *Bst*PI and the 3′ *Bam*H1 sites, and the digested products were subcloned into pT1-IRES-EGFP. The vectors of enhanced cyan fluorescent protein (ECFP)-Δ11 and ECFP-intracellular domain (ICD) were also prepared by PCR, using the 5′ primer GGTCTGCCGTCTGCACGTCTG and the 3′ primer of Δ11, CGCGGATCCTTAACCTTTCATGCC or the 3′ primer of ICD, CGCGGATCCCCCAGCCTTGTCTTTCCTTTATC. The deletion mutants are shown in Figure 3. The underlined sequences indicate the *Bam*H1 sites, and the boldface letters represent mutation sites. PCR was performed at 94°C for 30 s, 58°C for 30 s, and 72°C for 60 s for 30 cycles, followed by a final elongation at 72°C for 5 min with an Expand High Fidelity PCR system (Roche Applied Science). The amplified PCR products were separated on 2% agarose gel. The PCR products were digested by the 5′ and 3′ *Bam*H1 sites and were then subcloned into these sites of pECFP-C1 (Clontech). These constructs were transfected into HEK293 cells and astrocytes with Lipofectamine 2000.

Production of glutathione S-transferase-fusion proteins and in vitro binding assay. Constructs of glutathione *S*-transferase (GST)-fusion proteins were prepared by a PCR method. For the preparation of GST-T1-ICD, we used the above pT1-IRES-EGFP as a template, the 5′ primer CAAGAATTCCTCCAAGTTGGCGAGACATTCC, and the 3′ primer GTTGTCGACTTGTCTTTCCTTTATCTCAG. The single-underlined sequence indicates the *Eco*RI site, and the double-underlined sequence indicates the *Sal*I site. PCR was performed at 94°C for 30 s, 58°C for 30 s, and 72°C for 60 s for 25 cycles, followed by a final elongation at 72°C for 5 min with an Expand High Fidelity PCR system. The digested PCR product was subcloned into the pGEX-5X-3 bacterial expression vector

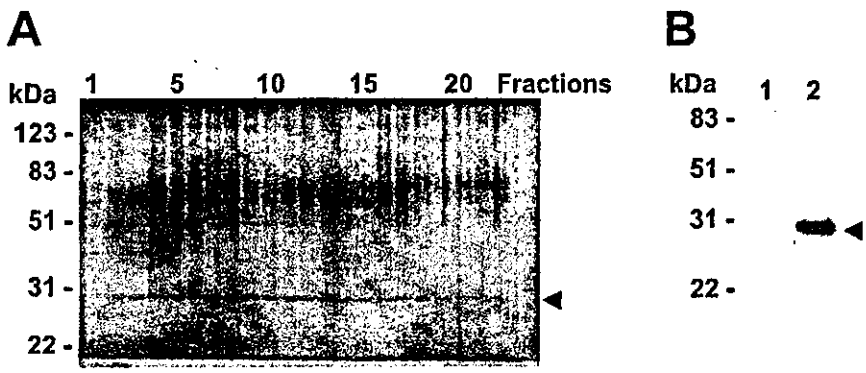

Figure 1. Affinity purification of a binding protein of T1. *A*, The cytosolic fraction from rat brain was loaded onto an affinity column with the T1 synthetic peptide. One-step elution with glycine (50 mM; pH 2.5) was performed, and elution samples from the column were separated; an aliquot of each eluate was subjected to SDS-PAGE (10% gel). The resulting silver-stained gel image is shown here. The arrowhead indicates the position of the 28 kDa protein. *B*, Western blot analysis of the eluate from the control column (lane 1) and the affinity column (lane 2) with anti-Rho GDI1. The arrowhead indicates the position of Rho GDI1 (28 kDa).

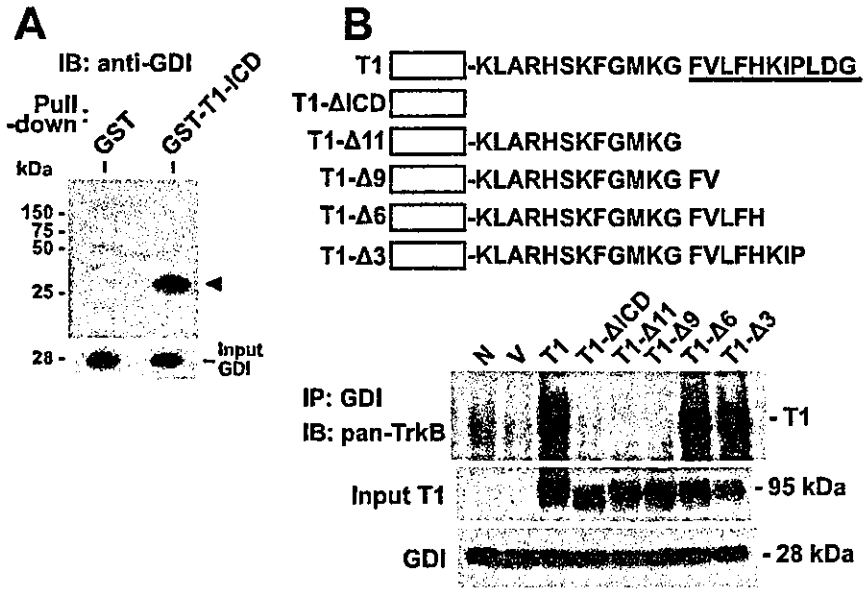

Figure 2. Direct binding of Rho GDI1 to T1 and binding motif in the T1-specific sequence. *A*, The GST moiety or the GST-T1-ICD was mixed with recombinant Rho GDI1 in Eppendorf tubes. The GST proteins were precipitated with glutathione-Sepharose 4B. The coprecipitated Rho GDI1 was detected with anti-Rho GDI1. The arrowhead indicates Rho GDI1 (28 kDa). *B*, The Rho GDI1 binding site in the intracellular domain of T1. A display of T1 and its deletion mutants is shown in the top panel. The white boxes represent the extracellular and transmembrane domains, and the underlined sequence indicates the specific amino acid sequence of T1. The constructs were transfected into HEK293 cells. After 24 h, coimmunoprecipitation with anti-Rho GDI1 was performed. N, No vector; V, empty vector expressing GFP; T1, normal T1; T1-ΔICD, T1 without its ICD; T1-Δn, T1 deletion mutants lacking the indicated number of amino acids from the C terminal. IB, Immunoblot; IP, immunoprecipitation.

(Amersham Biosciences, Piscataway, NJ). To obtain the cDNA of Rho GDI1, we used a cDNA library of the adult mouse cortex as a template, the 5′ primer CACGAATTCTAGGGCAGAACAGGACC, and the 3′ primer GTTGTCGACTAGGTAGGGGGTTAG. A single-underlined sequence indicates the *Eco*RI site, and a double-underlined sequence indicates the *Sal*I site. The boldface letter in the 5′ primer of GST-Rho GDI1 is the point mutation site. The methods used for PCR preparation and subcloning into the pGEX-5X-3 vector were the same as those used for T1. After the OD_{600} reached 0.6, 1 mM isopropyl-1-thio-β-D-galactopyranoside was added to the cultures, and *Escherichia coli* were grown for an additional 16 h at 25°C (Yamashita and Tohyama, 2003). After the cells were collected, they were resuspended in PBS and sonicated. To the cell lysates, 0.5% Triton X-100 was added, and the samples were incubated for 30 min at 4°C. After centrifugation at 10,000 × *g* for 5 min, glutathione-Sepharose 4B (Pharmacia, Piscataway, NJ) was added to the supernatants, which were then incubated for 30 min at 4°C. After centrifugation at 10,000 × *g* for 5 s, the beads were washed three times in PBS containing 0.5% Triton X-100. The purity of the proteins was determined by SDS-PAGE. Then, glutathione-Sepharose 4B with GST-T1-ICD was used for the binding assay. To remove the GST moiety from GST-Rho GDI1, Factor Xa (Novagen, Darmstadt, Germany) was added to the glutathione-Sepharose 4B with GST-Rho GDI1, and the samples were incubated for 16 h at 20°C. After centrifugation at 10,000 × *g* for 5 min, Xarrest agarose (Novagen) was added to the supernatants, and the samples were incubated for 10 min at room temperature. After centrifugation at 1000 × *g* for 5 min, the supernatants were designated as the recombinant Rho GDI1 without GST. To check the cleavage of GST-Rho GDI1, glutathione-Sepharose 4B was added into the supernatant of Rho GDI1, and the samples were incubated for 30 min at 4°C. After centrifugation at 10,000 × *g* for 5 min, the precipitates were washed three times in PBS containing 0.5% Triton X-100, and they were then boiled in SDS sample buffer (see supplemental Fig. 1, available at www.jneurosci.org as supplemental material).

For the *in vitro* binding assay, recombinant Rho GDI1 solution was added to the glutathione-Sepharose 4B with GST-T1-ICD, and the samples were incubated for 1 h at 4°C with agitation. After centrifugation at 10,000 × *g* for 5 s, the precipitates were washed three times in PBS containing 0.5% Triton X-100, and then they were boiled in SDS sample buffer.

Precipitation assays. After each incubation with reagents, the cells were lysed with 0.15 ml of lysis buffer. For Rho GDI1-T1 coimmunoprecipitation, lysis buffer A (10 mM triethanolamine, 10 mM iodoacetoamine, pH 7.8, 150 mM NaCl, 2 mM EDTA, 1% digitonin, 1 mM PMSF, 10 μg/ml leupeptin, and 20 μg/ml aprotinin) was used. The lysates were centrifuged at 10,000 × *g* at 4°C for 20 min. Then, 50 μl aliquots of resulting supernatants were designated as total protein samples. Normal mouse IgG and protein G-Sepharose were added to the remaining supernatants, which were incubated at 4°C for 1 h with gentle rotation. After centrifugation at 5000 × *g* at 4°C for 1 min, mouse monoclonal anti-pan-TrkB (2 μl; Transduction Laboratories, Lexington, KY) or rabbit polyclonal anti-Rho GDI1 (3 μl; Santa Cruz Biotechnology, Santa Cruz, CA) was added. In the competitive assays with the synthetic peptides of the T1 C terminal, the peptides (final concentration, 100 μM and 1 mM) were added to the lysates and incubated at 4°C for 1 h. The samples were incubated at 4°C for 2 h with antibody and then were incubated with protein G-Sepharose at 4°C for 1 h with gentle rotation. The precipitates were washed four times with lysis buffer A and boiled in 40 μl of SDS sample buffer for 3 min.

For the RhoA, Rac1, and Cdc42 pull-down assay, we used lysis buffer B [50 mM Tris-HCl, pH 7.5, 150 mM NaCl, 5 mM $MgCl_2$, 0.5% Triton X-100, 1 mM PMSF, 10 μg/ml leupeptin, 20 μg/ml aprotinin, and 10 nM microcystin LR (Leu and Avg)]. The lysates were centrifuged at 10,000 × *g* at 4°C for 20 min. We then performed the RhoA pull-down assay with Rhotekin beads (Upstate Biotech, Charlottesville, VA) according to the method of Ren et al. (1999) and the Rac1 and Cdc42 pull-down assay with p21-activated kinase (PAK) beads (Upstate Biotech). Then, the Rhotekin (Upstate Biotech) or PAK beads (30 μl) were added to the lysates (1 mg of protein/ml) and incubated at 4°C for 45 min. The beads

were washed three times with lysis buffer B. The pellets were then mixed with 40 μl of SDS sample buffer and boiled for 3 min. In the control assays using GTPγS- and GDP-loaded lysates, we confirmed our assay systems (supplemental Fig. 2, available at www.jneurosci.org as supplemental material). Briefly, 3 μl of 0.5M EDTA (10 mM) and then 1.5 μl of GTPγS (100 μM) or GDP (1 mM) was added to a 0.15 ml aliquot of each cell extract. The extracts were incubated at 30°C for 30 min. To stop the loading of GTPγS and GDP, we added 9 μl of 1 M $MgCl_2$ (60 mM). The procedures that were subsequently performed have been described above.

Western blot analysis. Using an aliquot of astrocytic culture lysates, we also performed a Western blot analysis of protein expression. The samples (5 μg total protein per lane, except for TrkB, Cdc42, and Rac1, as follows: 100 μg total protein per lane for TrkB, Cdc42, and Rac1 and 10 μl per lane for the precipitates) were subjected to SDS-PAGE and then were blotted onto PVDF membranes. The membranes were blocked for 1 h in 5% skim milk in PBS [containing (in mM): 137 NaCl, 8.1 $Na_2HPO_4 \cdot 7H_2O$, 2.7 KCl, and 1.5 KH_2PO_4]. After incubation with the primary antibodies at room temperature for 1 h, the blots were incubated for 1 h with secondary antibodies conjugated with HRP and then were visualized by the ECL system (Amersham Biosciences). For the primary antibodies, we used anti-pan-TrkB (1:200; Santa Cruz Biotechnology), anti-TK+ (1:200; Santa Cruz Biotechnology), anti-T1 (1:200; Santa Cruz Biotechnology), anti-RhoA (1:200; Santa Cruz Biotechnology), anti-Rac1 (1:1000; Transduction Laboratories), anti-Cdc42 (1:1000; Transduction Laboratories), anti-Rho GDI1 (1:200; Santa Cruz Biotechnology), and anti-β-tubulin (1:1000; Sigma).

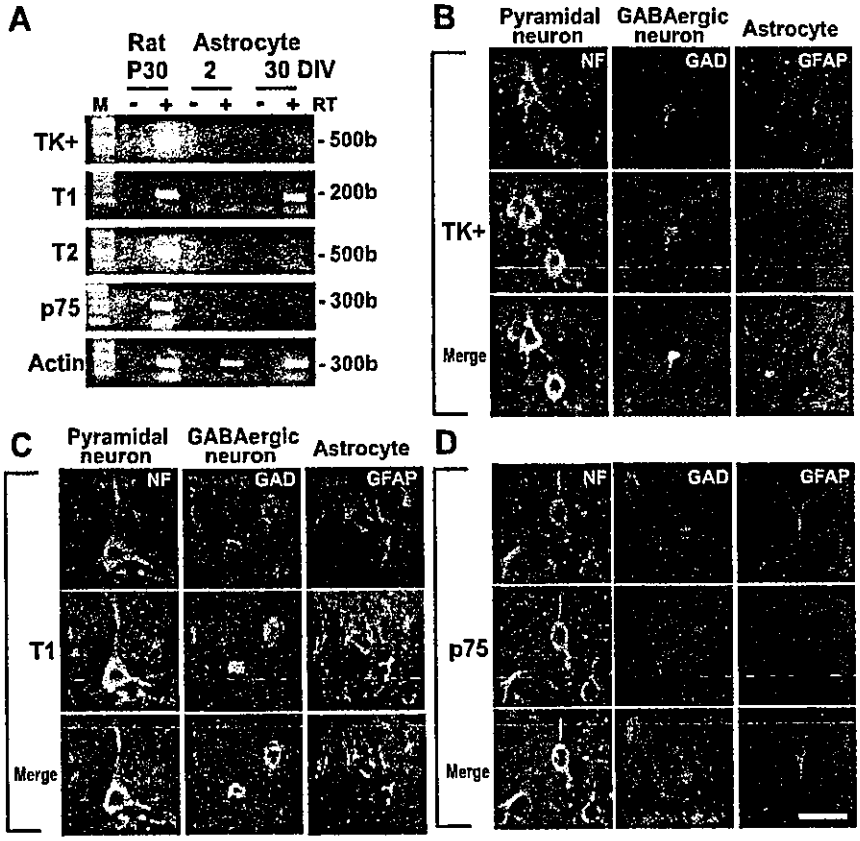

Figure 3. Expression of BDNF receptors in astrocytes in primary culture and young adult rat brain. *A*, RT-PCR analysis of TrkB subtypes and p75 expression in P30 rat neocortex and astrocytes at 2 and 30 DIV. M, 100 base marker. *B–D*, Distributions of TK+, T1, and p75 in the young adult (4-week-old) rat cortex. Astrocytes in layers I/II, pyramidal neurons, and GABAergic neurons in layers V/VI of the motor cortex are represented. Pyramidal neurons, GABAergic neurons, and astrocytes immunostained using anti-neurofilament (NF), anti-GAD (GAD), and anti-GFAP (GFAP), respectively, are shown in red. The immunopositive structures of TK+, T1, and p75 are shown in green. The double-positive cells in the merged images are shown in yellow-green. Scale bar, 20 μm.

Immunohistochemistry. Young adult rats (4-week-old Wistar rats) were anesthetized and perfused with 4% formaldehyde in phosphate buffer. The brains were postfixed for 6 h and cryoprotected in 30% sucrose in PBS. The brains were mounted in Tissue-Tek (Miles, Elkhart, IN), frozen rapidly on dry ice, and stored at −30°C. The sections were cut to a thickness of 35 μm with a cryostat (Leica, Wetzlar, Germany). The sections were mounted on glass slides coated with 3-aminopropyltriethoxysilane, washed for 30 min with PBS, and then preincubated with PBS-GB [4% normal goat serum (Vector Laboratories, Burlingame, CA) and 1% bovine serum albumin in PBS] for 2 h at room temperature. The sections were incubated for 48 h at 4°C with antibodies. We used the following primary antibodies: rabbit polyclonal anti-TK+ (1:800) and anti-T1 (1:800) and mouse monoclonal anti-neurofilament (1:1000; clone SMI32; Sternberger Monoclonals, Lutherville, MD), anti-glutamic acid decarboxylase (GAD; 1:3000; Affinity Research Products, Exeter, UK), and anti-glial fibrillary acidic protein (GFAP; 1:1000; Chemicon, Temecula, CA). The sections were incubated for 1 h at room temperature with the following secondary antibodies: anti-mouse IgG cyanine 3 (Cy3; 1:200; Chemicon) and anti-rabbit IgG Alexa 488 (1:200; Molecular Probes, Eugene, OR). The sections were embedded with Permafluor (Thermo Shandon, Pittsburgh, PA). We used a confocal microscope (TCS SP2; Leica) to analyze the samples.

Morphological assays. The cells were stimulated for the indicated periods at 37°C with 20 ng/ml BDNF (PeproTech, Rocky Hill, NJ) or 100 ng/ml NGF (PeproTech) or vehicle. The cell samples were also incubated for 20 min with anti-BDNF (5 μg/ml; Santa Cruz Biotechnology) and then were incubated for 30 min with 20 ng/ml BDNF. For treatment with Toxin A (Biogenesis, Poole, UK) and C3 toxin (Calbiochem, La Jolla, CA), we performed the procedures according to methods described previously (Just et al., 1995; Maekawa et al., 1999). Toxins (20 ng/ml of Toxin A, 30 μg/ml of C3 toxin) were added to the 30 DIV cells, and the cells were incubated for 24 h at 37°C. The cells were washed twice in PBS and then were fixed in 4% formaldehyde in PBS for 1 h at room temperature. The cells were preincubated with PBS-GB and were incubated with anti-GFAP for 48 h at 4°C. After being washed in PBS, the cells were incubated with anti-mouse IgG Cy3. The cells were then embedded with Permafluor. We used a confocal microscope for the analysis. For the time-lapse analysis, the astrocytic cultures were set on the confocal microscope (TCS SP2; Leica) with oxygen supply. Phase-contrast images were taken using a 40× water-immersion objective at indicated time. Each cell area was measured by AquaCosmos (Hamamatsu Photonics K.K., Hamamatsu, Japan).

Results

Rho GDI1 is a T1-binding protein

T1 exhibits a characteristic developmental expression pattern in the mammalian CNS (i.e., the expression of T1 is known to be remarkably increased after birth and is a major product among TrkB subtypes in adults) (Allendoerfer et al., 1994; Fryer et al., 1996; Ohira et al., 1999). Thus, we purified T1-binding proteins from the cytosolic fraction of adult rat brains, using an affinity column conjugated with the C-terminal-specific sequence of T1. A 28 kDa protein was eluted from the column as a sharp peak under low pH conditions using glycine buffer, pH 2.5 (Fig. 1*A*). The fractions containing the protein eluted from the affinity column were concentrated by a centrifugal concentrator. Then, the 28 kDa protein was purified as a single band blotted on a PVDF membrane and cleaved by CNBr. The resulting peptides were

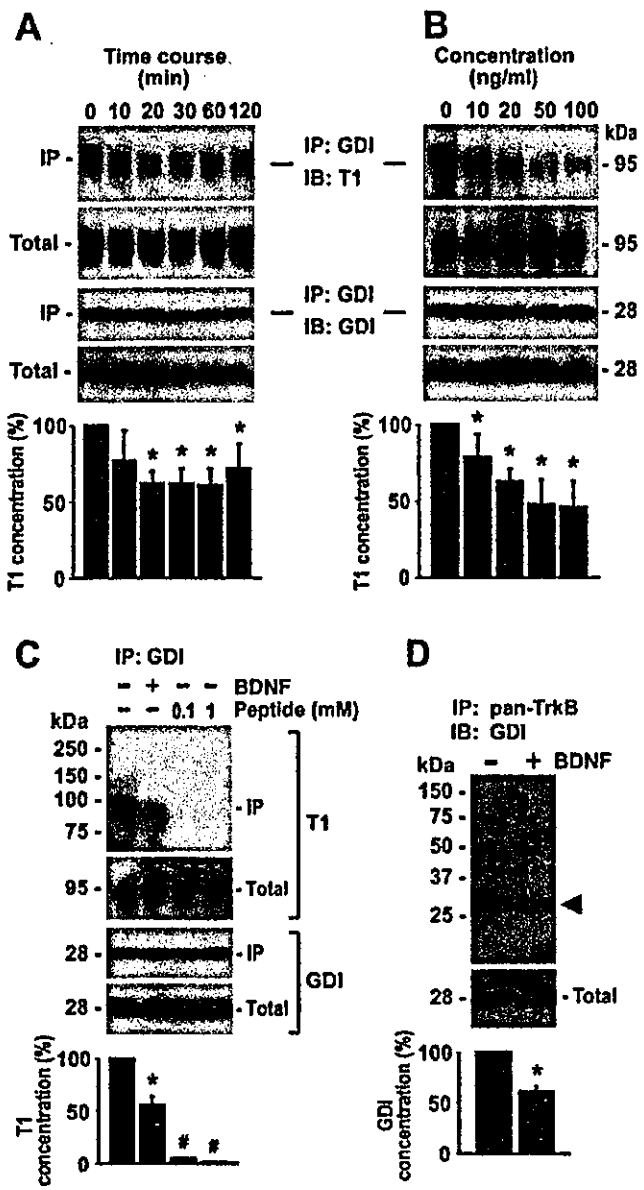

Figure 4. Dissociation of Rho GDI1 from T1 by BDNF treatment in 30 DIV astrocytes. *A*, Coimmunoprecipitation of T1 with anti-Rho GDI1 at each time point after BDNF stimulation (20 ng/ml). *B*, Ligand-concentration dependency of the interaction between T1 and Rho GDI1 at 30 min after each concentration of BDNF stimulation. *C*, Competitive assay using the T1-specific peptides. The synthetic peptides of the T1 C terminal were added to the lysates of 30 DIV astrocytes. At the concentration of 100 μM and 1 mM, the T1 bands were hardly observed (lanes 3 and 4). *D*, Coimmunoprecipitation of Rho GDI1 with anti-pan-TrkB. Astrocytes were stimulated for 30 min by BDNF (20 ng/ml). The arrowhead indicates Rho GDI1 (28 kDa). Quantitative analysis of the bands in *A–D*. The control levels were taken as 100%. The asterisks indicate statistically significant differences ($p < 0.05$; one-way ANOVA and Scheffé's *post hoc* test). In *C*, the # symbol indicates significant differences between the BDNF and the peptide treatments ($p < 0.05$; one-way ANOVA and Scheffé's *post hoc* test). Values are given as means ± SD of four independent experiments. IB, Immunoblot; IP, immunoprecipitation.

separated by gel electrophoresis and blotted on a PVDF membrane to purify each band. The N-terminal sequence of one peptide was determined as KYIQHT according to the Edman degradation method. Consequently, this sequence was found to match the inner sequence of Rho GDI1, a Rho guanine nucleotide dissociation inhibitor that can stabilize the inactive, GDP-bound form of Rho GTPase (Takai et al., 2001). Western blot analysis identified the 28 kDa protein as Rho GDI1 (Fig. 1*B*).

In vitro binding assay

To examine whether T1 directly binds to Rho GDI1, we performed an *in vitro* pull-down assay using recombinant proteins (i.e., the GST-T1-ICD and Rho GDI1). As shown in Figure 2*A*, the GST moiety did not bind to Rho GDI1, whereas the GST-T1-ICD fusion protein precipitated Rho GDI1. The possible contribution of the direct binding of GST-Rho GDI1 to glutathione-Sepharose 4B as a result of incomplete cleavage could be excluded, because we detected the Rho GDI1 at 28 kDa but not the 54 kDa band of the fusion protein. Therefore, we concluded that T1 directly binds to Rho GDI1.

Binding motif of T1 with Rho GDI1

We further determined a specific motif of T1 binding to Rho GDI1 using deletion mutants of the C terminal of T1. Constructs of T1 lacking its intracellular domain (T1-ΔICD) and T1 deletion mutants lacking the indicated number of amino acids from the C-terminal domain (T1-Δn) were transfected into HEK293 cells, and coimmunoprecipitation with anti-Rho GDI1 antibody was performed at 24 h after transfection. We detected the bands of both T1-Δ3 and T1-Δ6 at ~95 kDa, which was comparable with those of normal T1 (Fig. 2*B*). However, deletion mutants lacking nine or more amino acids were no longer able to bind to Rho GDI1. Thus, the present results suggested that LFH in the T1-specific sequence (FVLFHKIPLDG) is responsible for binding to Rho GDI1.

Expression of BDNF receptors in astrocytic primary cultures and adult rat brains

T1 has been reported to be distributed in both neurons and glia (Frisén et al., 1993; Armanini et al., 1995; Ohira and Hayashi, 2003). In astrocytic primary cultures from the neonatal rat hippocampus, RT-PCR analysis did not reveal the mRNA expression of any of the TrkB subtypes or of p75 at 2 DIV after plating (Fig. 3*A*). Astrocytes cultured long-term (30 DIV) expressed T1 mRNA, whereas no TK+, T2, or p75 mRNA expression was detected. We also examined the distribution of T1 in the adult rat cortex using fluorescent double-staining histochemistry. In this series, the following cell markers were used: neurofilament for pyramidal neurons, GAD for GABAergic neurons, and GFAP for astrocytes. TK+ immunoreactivity was localized in both pyramidal and GABAergic neurons but not in astrocytes (Fig. 3*B*). In contrast, T1 immunoreactivity was detected not only in both pyramidal and GABAergic neurons, but also in the astrocytes (Fig. 3*C*). The neurotrophin receptor p75 (p75) was only expressed in the pyramidal neurons (Fig. 3*D*). Together, these results indicate that astrocytes in the cortex and hippocampus of adult rats possess only T1 among the known BDNF receptors. Therefore, we used rat hippocampal astrocytes to investigate the signaling mechanism of T1.

Dissociation of Rho GDI1 from T1 in a BDNF-dependent manner

To determine whether Rho GDI1 dissociated from T1 in a BDNF-dependent manner in long-term cultured (30 DIV) astrocytes, we performed a pull-down assay of T1 with anti-Rho GDI1 antibody, and we detected T1 using anti-T1 antibody. As shown in Figure 4*A*, the T1 band was reduced to ~60% of the control level at 20 min after BDNF treatment (20 ng/ml). The reduced levels of T1 bands were maintained for 60 min, and then a less significant reduction in T1 bands (70% of the control level) was observed at 120 min after the addition of BDNF. Moreover, the dissociation of Rho GDI1 from T1 appeared to occur in a dose-

dependent manner (Fig. 4*B*). We found that 50 ng/ml BDNF stimulation for 30 min led to the adequate dissociation of Rho GDI1, which then reached a plateau level (50% of control level).

Furthermore, to determine whether the interaction between T1 and Rho GDI1 was specific, we performed the peptide competition assays using the T1-specific C-terminal peptide. The peptides were added to the lysates derived from 30 DIV astrocytes to a final concentration of 100 μM or 1 mM. Both additions of 100 μM and 1 mM peptides significantly inhibited the interaction (4.7 and 1.4% of control level, respectively) (Fig. 4*C*). Because Rho GDI1 was immunoprecipitated by anti-Rho GDI1 in the competitive assays (Fig. 4*C*, lanes 3 and 4), which was comparable with the control level (Fig. 4*C*, lane 1), the peptides specifically blocked the T1 binding to Rho GDI1.

In addition, we performed a pull-down assay of Rho GDI1 using anti-pan-TrkB antibody, and we detected Rho GDI1 using anti-Rho GDI1 antibody; this approach thus reversed the use of the antibodies to confirm the interaction between T1 and Rho GDI1. Then, we found that the Rho GDI1 band was reduced by 60% of the control level by BDNF treatment (Fig. 4*D*), which was comparable with the results of the pull-down assay performed with anti-Rho GDI1. Therefore, these findings suggest that treatment with BDNF can lead to the dissociation of Rho GDI1 from T1. In the subsequent experiments, to obtain sufficient dissociation of Rho GDI1 from T1, we applied 20 ng/ml BDNF for 30 min to astrocytic cultures. At the concentration of 20 ng/ml BDNF, p75 cannot function (Dechant and Barde, 1997), even through p75 expression remained below the levels that could be detected by PCR (Fig. 3*A*).

BDNF effects on astrocytic morphology in 30 DIV cultures

Rho GTPases are involved in the regulation of cell morphology by remodeling the cytoskeleton, which contains microfilaments, intermediate filaments, and microtubules (Ridley, 2001; Etienne-Manneville and Hall, 2002). Rho GDI1 has been shown to selectively interact with the GDP-bound forms of the Rho GTPases and to inhibit their conversion from the GDP-bound inactive form to the GTP-bound active form (Takai et al., 2001). Thus, we examined the morphological alteration of astrocytes by endogenous T1 in 30 DIV cultures. In serum-free medium containing N2 supplement, the form of 30

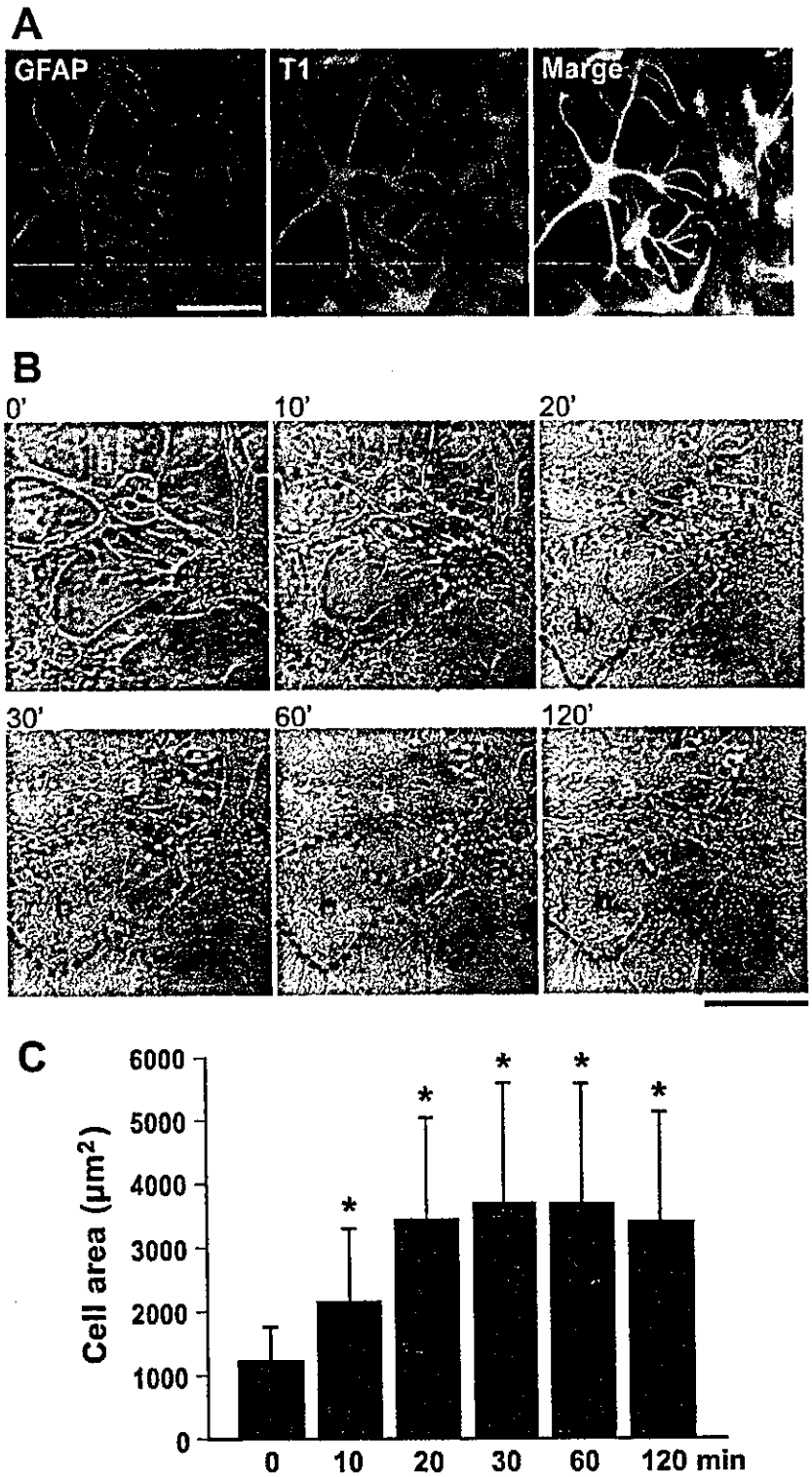

Figure 5. Morphological changes in astrocytes in 30 DIV astrocytic cultures. *A*, Coexpression of GFAP and T1 in the 30 DIV astrocytes. The cells were incubated in DMEM containing N2 supplement without BDNF stimulation and fixed in 4% formaldehyde. The immunoreactive cells for GFAP and T1 were stained by red and green, respectively. The cells coexpressing both GFAP and T1 were yellow. Note that almost all cells were coimmunopositive. Scale bar, 50 μm. *B*, Time-lapse images of the 30 DIV astrocytic cultures by the phase-contrast microscope. BDNF (20 ng/ml) was added to the 30 DIV cultures at 0 min. The number in each photograph indicates the time lapse (in minutes) after BDNF treatment. Three cells were marked by the colored small letter, yellow "a," red "b," and black "c," and they were also outlined by the dotted lines of corresponding colors. Note that the more the time passed, the thinner the cell bodies and processes were. Scale bar, 20 μm. *C*, Quantification of cell size. Values are given as the means ± SD of the cell size analysis based on the results of four independent experiments (total cell counts: 0 min, $n = 944$; 10 min, $n = 1003$; 20 min, $n = 978$; 30 min, $n = 981$; 60 min, $n = 1105$; 120 min, $n = 1054$). The asterisks indicate significant differences ($p < 0.05$; one-way ANOVA and Scheffé's *post hoc* test) compared with the value at 0 min.

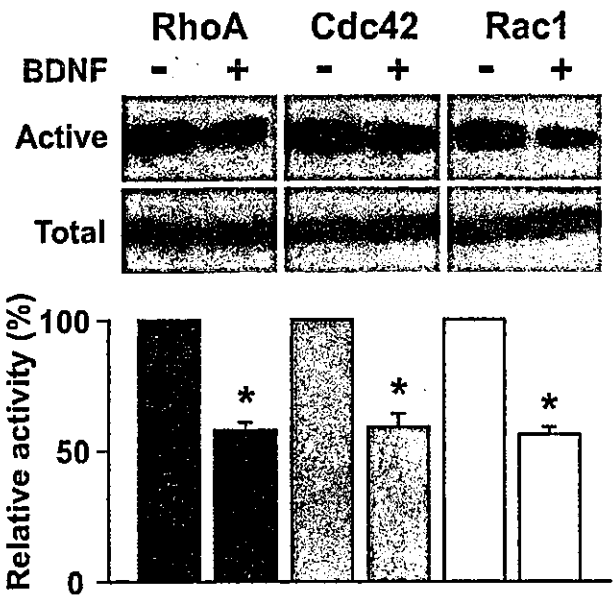

Figure 6. Activities of Rho GTPases in 30 DIV astrocytic cultures. Top, The cells were stimulated for 30 min with BDNF (20 ng/ml), and the cell extracts were subjected to *in vitro* binding assays. The precipitates and total proteins (5 μg for RhoA; 100 μg for Cdc42 and Rac1) were loaded on 15% gel and were detected with specific antibodies. Bottom, Quantitative analysis of the bands shown in the above images. Each control level, without BDNF stimulation, was taken as 100%. The asterisks indicate statistically significant differences ($p < 0.05$; paired Student's *t* test). Values are given as means ± SD of four independent experiments.

DIV astrocytes became fibrous (Fig. 5*A*,*B*). Almost all astrocytes were immunoreactive for both GFAP and T1 (Fig. 5*A*). The time-lapse analysis showed that BDNF stimulation led to a dynamic change in the shape of the astrocytes from fibrous to flat within 30 min (Fig. 5*B*). The cell surface area significantly increased 1.7-fold at 10 min and reached a threefold plateau level at 30 min (Fig. 5*C*). At 120 min after BDNF stimulation, the cells had decreased in size, albeit not significantly. At the same time, we measured the activities of RhoA, Rac1, and Cdc42, which are substrates of Rho GDI1, at 30 min when the change in astrocytic morphology reached a maximum. The active forms of all Rho GTPases were reduced by 60% of the control level (Fig. 6). The observed alterations in the shape of the astrocytes and the changes in Rho GTPase activity were both closely associated with the interaction between T1 and Rho GDI1 (Fig. 4), suggesting that BDNF-T1-Rho GDI1 signaling might control the Rho GTPases and consequently alter astrocytic morphology.

To elucidate the mechanism by which Rho GTPases regulate astrocytic morphology, we performed an inhibition assay of Rho GTPases using Toxin A and C3 toxin, which are known to inhibit all Rho GTPases (RhoA, Cdc42, and Rac1) and RhoA, respectively, in 30 DIV cultures. The astrocytic cultures were stimulated by BDNF at 20 ng/ml for 30 min. The results of the control cells were the same as the time-lapse analysis above (Fig. 7*A*). The astrocytes without BDNF treatment had long processes. Being treated by BDNF, the shapes of astrocytes were flat. In the Toxin A-treated cultures, the morphology of astrocytes was flat, regardless of BDNF treatment (Fig. 7*A*), which was similar to the shapes of the BDNF-treated control cells. The size of the cells was the same as that of BDNF-treated normal astrocytes (Fig. 7*B*). In contrast, C3 toxin treatment left the astrocytic morphology fibrous with fine filopodia-like processes (Fig. 7*A*). After BDNF treatment, the cells flattened; these findings were comparable with the observed morphology and size of the BDNF-treated control cells and the Toxin A-treated cells (Fig. 7*A*). Therefore, endogenous T1 might alter astrocytic morphology (i.e., it renders astrocytes fibrous and flat) via the control of Rho GTPases and primarily through Cdc42 and Rac.

Involvement of T1 in the regulation of astrocytic morphology

We examined the molecular mechanism of the T1-induced morphological alteration of astrocytes by performing a transfection assay with T1 mutants. Because 30 DIV astrocytes were refractory to transfection (<5%), whereas short-term cultured astrocytes (2 DIV) were easily transfected at high transfection efficiencies (>90%), we used 2 DIV astrocytes, in which we observed no expression of BDNF receptors (Fig. 3*A*).

First, we examined the effect of BDNF on the morphology of astrocytes overexpressing normal T1 or a T1 deletion mutant. Both the untransfected control cells and empty vector (GFP)-transfected cells showed a flat polygonal morphology with processes (Fig. 8). When these cells were treated with BDNF (20 ng/ml) for 30 min, we observed no changes in the cell morphology. On the other hand, the T1-transfected cells exhibited a fibrous, spindle morphology with long and narrow processes, even under the no-treatment condition. Interestingly, BDNF treatment rapidly and remarkably altered the cell morphology. Only 30 min after treatment with BDNF, the cells exhibited flat and wide cell bodies and stretched-out GFAP-positive fibers. The relative cell area of T1-transfected astrocytes treated with BDNF increased significantly, about fivefold, compared with that of T1-transfected astrocytes without BDNF treatment (Fig. 8*B*). In contrast, when T1-Δ11, a deletion mutant of a T1-specific sequence (Fig. 2*B*), was transfected, the cell morphology observed was a flat polygon with processes similar to those of the control, and BDNF treatment was not found to induce any morphological changes such as those found in the T1-transfected cells. Recently, p75 has been reported to associate with Rho GDI1 and regulate Rho activity (Yamashita et al., 1999; Yamashita and Tohyama, 2003). However, high-concentration treatment with NGF (100 ng/ml), which is a p75 ligand, had no effect on cell morphology. Taken together with the evidence that there was no morphological change in nontransfected cells or in GFP-expressing cells, it was concluded that p75 had no effect on cell morphology.

Next, we investigated whether BDNF negatively regulates the Rho GTPases through Rho GDI1 released from T1. To this end, we performed a pull-down assay of the active forms of the Rho GTPases. In astrocytes expressing exogenous T1, BDNF treatment was found to reduce the amount of activated RhoA, Cdc42, and Rac1 by 55, 51, 55% of the control level, respectively (Fig. 9). In contrast, cells expressing T1-Δ11 and cells treated with NGF (100 ng/ml) were not associated with a decrease in the active forms of RhoA, Cdc42, and Rac1. These results are compatible with findings regarding the regulation of Rho GTPase activity by endogenous T1 (Fig. 6). Thus, the present results suggest that the specific C-terminal alignment of T1 is necessary for the control of Rho GTPases and for the observed morphological alteration of astrocytes.

Competitive assay with T1 intracellular peptides

We then investigated the effects of the T1-specific C-terminal peptide on the regulation of astrocytic morphology. To inhibit the T1 signaling cascade in a competitive manner, we cotransfected the expression vectors of T1 and each of the following: CFP, CFP-Δ11, and CFP-ICD. We expected that CFP-ICD, but not CFP or CFP-Δ11, would trap Rho GDI1 within the cytoplasmic region and inhibit the association of Rho GDI1 to the Rho

GTPases, thereby resulting in the inhibition of the activity of BDNF. As shown in Figure 10, *A* and *B*, when both CFP and CFP-Δ11 were transfected with normal T1, we observed fibrous astrocytes under the condition lacking BDNF treatment. The addition of BDNF induced the morphological alteration of the astrocytes from fibrous to flat for 30 min. Namely, neither CFP nor CFP-Δ11 blocked the effects of BDNF, compared with the results obtained with the transfectant with T1-expression vector alone (Fig. 8). On the other hand, when CFP-ICD was overexpressed, the cells exhibited the same fibrous characteristics as were observed in the cases of the CFP- and CFP-Δ11-transfected cultures. However, BDNF treatment was not found to induce morphological changes among the astrocytes that remained fibrous. Therefore, the T1-specific sequence was determined to be indispensable for the morphological alteration of these astrocytes.

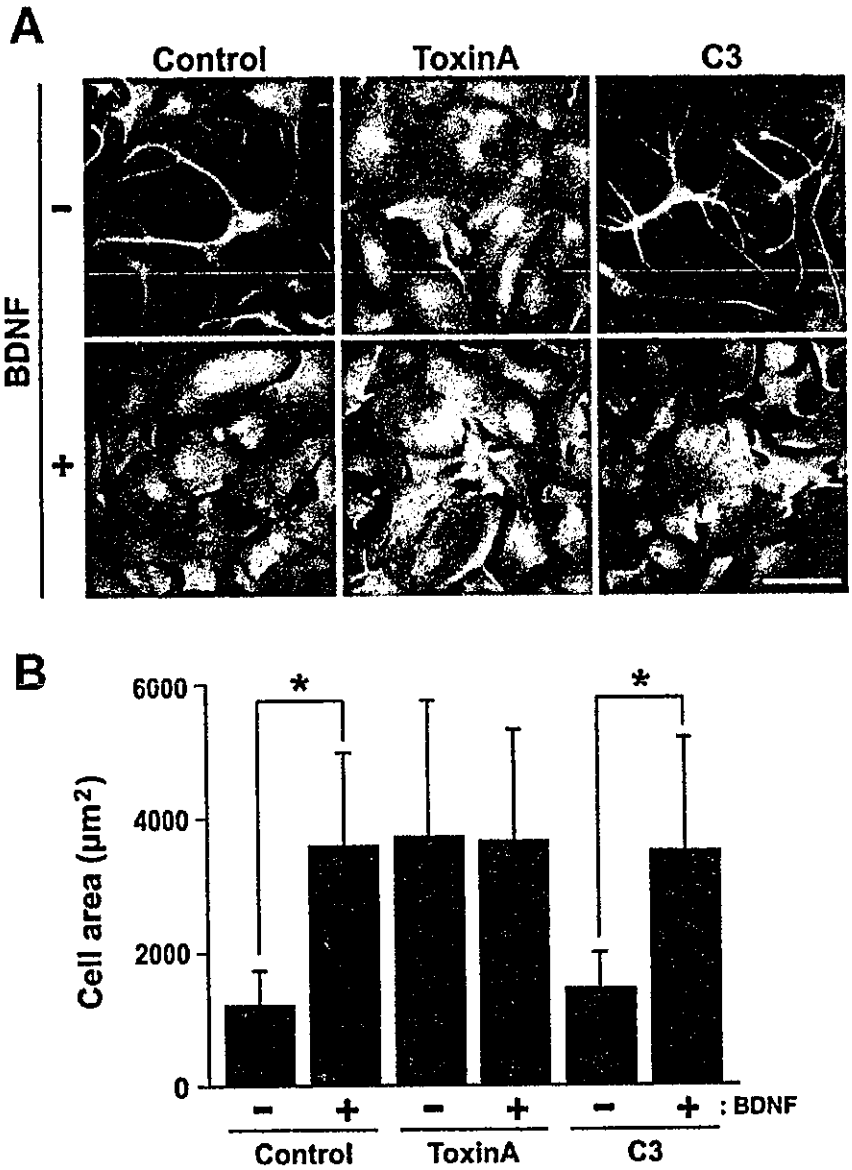

Figure 7. Morphological changes in astrocytes treated with Toxin A and C3 in 30 DIV astrocytic cultures. *A*, The images of cells treated by nothing (control), Toxin A, and C3. The 30 DIV astrocytes were incubated with Toxin A (20 ng/ml) or C3 (30 μg/ml) for 24 h. After being washed with serum-free medium, BDNF (20 ng/ml) was added to the cells, which were then fixed in 4% formaldehyde. The cells were stained with anti-T1 (green) and anti-GFAP (red). All displays show merged images (yellow). Scale bar, 50 μm. *B*, Quantitative analysis of cell size. Values are given as means ± SD of four independent experiments (total cell counts: control, without BDNF, $n = 914$, with BDNF, $n = 991$; Toxin A, without BDNF, $n = 948$, with BDNF, $n = 1064$; C3, without BDNF, $n = 1055$, with BDNF, $n = 1072$). The asterisks indicate statistically significant differences ($p < 0.05$; paired Student's *t* test).

Discussion

In the present study, we demonstrated that (1) a truncated TrkB receptor, T1, is capable of ligand-mediated signaling via Rho GDI1, which acts as a negative inhibitor in the Rho signaling cascade, and (2) the T1 signaling cascade regulates glial cellular morphology. A schematic representation is shown in Figure 10*C*. Our findings clearly indicate that T1 is not only the dominant-negative form of TK+, but is also the active receptor of BDNF itself.

Interaction between T1 and Rho GDI1

The *in vitro* binding analysis clearly showed the direct binding of Rho GDI1 and T1 (Fig. 2). One would question what fraction of T1 and Rho GDI1 contributes to the association between T1 and Rho GDI1. In the Western blot analysis in Figure 4, we loaded the 100 μg total protein per lane for TrkB, which is approximately one-third amount of total protein in each lysate derived from a 3 cm dish. As shown in Figure 4*A–C*, the level of the precipitated T1 in the control (at 0 min or no addition of BDNF) is comparable with the total level. In addition, in this study, the immunoprecipitations with anti-GDI or anti-pan-TrkB were performed with an efficiency of ~30%. The one-fourth of each precipitate was loaded on SDS-PAGE. Therefore, 44% of total T1 in an astrocyte bind to Rho GDI1.

In Figure 4*D*, ~1/50 amount of total protein in each lysate (5 μg total protein per lane) for Rho GDI1 was loaded on each lane. As described above about T1, we calculated the fraction of Rho GDI1 in the interaction between T1 and Rho GDI1. Consequently, ~2.2% of total Rho GDI1 in an astrocyte is involved in the binding to T1. It is a big surprise for us that the drastic change of astrocytic morphology is attributable to the low percentage of Rho GDI1 associating with T1. Rho GTPases are implicated in the important cell functions via remodeling cytoskeleton such as proliferation, migration, elongation of neurites, and membrane trafficking, suggesting that Rho GTPases are strictly regulated. Therefore, Rho GDI1 as a regulator of Rho GTPases are also severely controlled. Then, Rho GDI1 regulated by T1 may be small amount. A part of the rest of Rho GDI1 may be interacted with ERM consisting of ezrin, radixin, and moesin (Sasaki and Takai 1998) and might be bound to other unknown proteins.

Interaction between T1 and other proteins

p75 has been reported to control the activity of RhoA in a Rho GDI1-dependent manner (Yamashita et al., 1999; Yamashita and Tohyama, 2003). In the present study, we demonstrated that T1 also binds directly to Rho GDI1 and that LFH residues in the T1-specific sequence is important for this type of binding. Be-

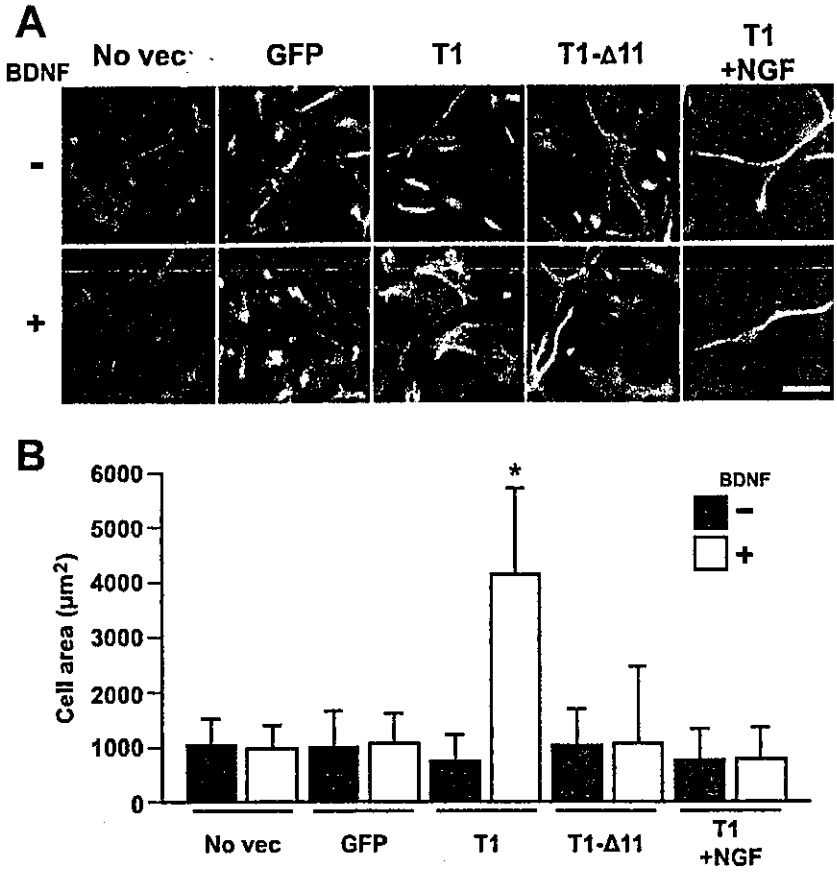

Figure 8. Morphological changes in astrocytes in 2 DIV cultures. *A*, No Vec, No transfection; GFP, EGFP; T1, normal T1; T1-Δ11, a deletion form of the T1-specific sequence (see Fig. 2*B*); T1 + NGF, normal T1-expressing cells that were treated with 100 ng/ml NGF instead of with BDNF. The cells were stimulated with vehicle (−) or with 20 ng/ml BDNF (+) and then were stained with anti-GFAP. Almost all of the cells were double positive for GFP (green) and GFAP (red), except for the No Vec cells. All displays show merged images (yellow-green). Scale bar, 30 μm. *B*, Quantification of cell size in *A*. Values are given as the means ± SD from the results of four independent experiments (total cell counts: No Vec, without BDNF, $n = 854$, with BDNF, $n = 821$; GFP, without BDNF, $n = 879$, with BDNF, $n = 787$; T1, without BDNF, $n = 698$, with BDNF, $n = 731$; T1-Δ11, without BDNF, $n = 687$, with BDNF, $n = 634$; T1 + NGF, without BDNF, $n = 810$, with BDNF, $n = 834$). The asterisks indicate significant differences ($p < 0.05$; one-way ANOVA and Scheffé's *post hoc* test) from the values obtained without BDNF treatment.

cause LFH is not contained in the intracellular domain of p75, both T1 and p75 may bind different regions of Rho GDI1.

Recently, Kryl and Barker (2000) reported that truncated TrkB-interacting protein (TTIP) is isolated from 15N neuroblastoma cells by using coimmunoprecipitation with GST fusion protein containing the intracellular juxtamembrane. TTIP has a molecular weight of 61 kDa, and T1 peptide competitively interrupted TTIP binding to T1, suggesting the direct binding interaction between them. However, the BDNF stimulation cannot modulate the interaction between T1 and TTIP. Kryl and Barker (2000) also analyzed TTIP by using matrix assisted laser desorption/ionization-mass spectrometry and described that TTIP is an unique protein. It is uncertain whether Rho GDI1 and TTIP bind directly to the different motifs in the T1-specific region or compete the same binding site. T1-mediated signaling may depend on its cellular compartment, because a fraction of T1 binds Rho GDI1. On the other hand, we detected proteins of 50, 60, and 72 kDa eluted from an affinity column (Fig. 1*A*); however, the correlation of each of these proteins with TTIP remains to be clarified.

Regulation of Rho proteins and astrocytic morphology by T1

The T1-interacting protein, Rho GDI1, is an inhibitory regulator of the Rho GTPases: Rho GDI1 is able to inhibit the activation of RhoA, Cdc42, and Rac1. On the other hand, the Rho GTPases are involved in the remodeling of the actin cytoskeleton: RhoA is involved in the formation of stress fibers; activated Cdc42 and Rac1 lead to lamellipodia and cell spreading, whereas activated Cdc42 induces filopodia (Hall, 1998). In this study, we demonstrated that Rho GDI1 released from T1 decreased the activities of the Rho GTPases, RhoA, Cdc42, and Rac1. However, it has remained unclear which Rho protein is related to the morphological changes in astrocytes triggered by BDNF. All Rho GTPases are known to be inhibited by Toxin A, and the form of astrocytes treated with Toxin A became flat. In contrast, the addition of C3, an inhibitor of RhoA, led to the formation of fibrous astrocytes with fine processes. Therefore, we were able to distinguish at least three types of morphology in this experiment. In the first type, the astrocytes became flat when all Rho GTPases were inhibited (Toxin A in Fig. 7*A*). In the second type, when only RhoA was inhibited by C3, the morphology of the cells was fibrous (C3 in Fig. 7*A*), which differed from the morphology of 30 DIV cells before the addition of BDNF (at 0 min in Fig. 5*A* and control in Fig. 7*A*), and the morphology of the fibrous cells also differed from that of T1-expressing 2 DIV cells (T1 in Fig. 8*A*). In the C3-treated condition, the processes of the astrocytes resembled filopodia; that is, fine processes extended from the bold processes of the astrocytes and the cell bodies (C3 in Fig. 7*A*). In the third type, the cells were not as fibrous as the second type of cell when the activities of the Rho GTPases remained at their basal levels. Typically, 30 DIV and T1-overexpressing astrocytes had spindle-shaped bodies or small, flat cell bodies and long processes (Figs. 5*A*, 7*A*, 8*A*). Thus, it appears that BDNF-T1 signaling suppressed the activity of all three Rho proteins and then induced morphological change leading to the flat type 1 cells. In addition, the cell flattening appears to be mediated primarily by the suppression of Cdc42 and Rac. In this context, it should be emphasized that extension of the astrocyte cell bodies was observed as a result of the inhibition of the Rho GTPases by T1-Rho GDI1 signaling. Recent studies have shown that the Rho GTPases control the remodeling of microfilaments, intermediate filaments, and microtubules (Ridley, 2001; Etienne-Manneville and Hall, 2002). Therefore, the regulation of cell morphology is not solely dependent on the microfilaments but instead depends on the well orchestrated control of various cytoskeletal proteins. More precise information regarding the mechanism of their regulation by BDNF remains to be obtained by additional study.

Functional role of T1 in astrocytes

In the present study, we demonstrated that astrocytes are able to alter their morphology rapidly and dramatically via the T1 > Rho GDI1 > Rho GTPase signaling cascade in a BDNF-dependent manner. In the mature mammalian CNS, BDNF is synthesized and secreted from presynaptic and/or postsynaptic sites, depend-

ing on neural activity (Fawcett et al., 1998; Aloyz et al., 1999; Hartmann et al., 2001; Kohara et al., 2001). Thus, astrocytic morphological changes might take place in an activity-dependent manner. On the other hand, recent studies have reported that glial morphology is drastically altered to maintain the clearance of neurotransmitters and to maintain the neural network and neural plasticity (Iino et al., 2001; Oliet et al., 2001; Hirrlinger et al., 2004). In addition, calcium entry into astrocytes has been assumed to be important for the modulation of synaptic transmission (Araque et al., 1999). More recently, T1 has been shown to mediate BDNF-induced calcium signaling in astrocytes (Rose et al., 2003; for review, see Kovalchuk et al., 2004). Although it remains unclear whether or not the entry of calcium into astrocytes can induce the alteration of astrocytic morphology, a mechanism involving the Rho GTPases might be associated with the entry of calcium into astrocytes (Illenberger et al., 1998; Ghisdal et al., 2003; Mehta et al., 2003). Thus, morphological changes attributable to the T1 signaling cascade in astrocytes surrounding synapses may modulate neuron–glial interactions as well as local calcium buffering effects, which would eventually lead to rapid changes in synaptic transmission. The relationship between the T1 signaling cascade and the entry of calcium into astrocytes appears to require additional examination.

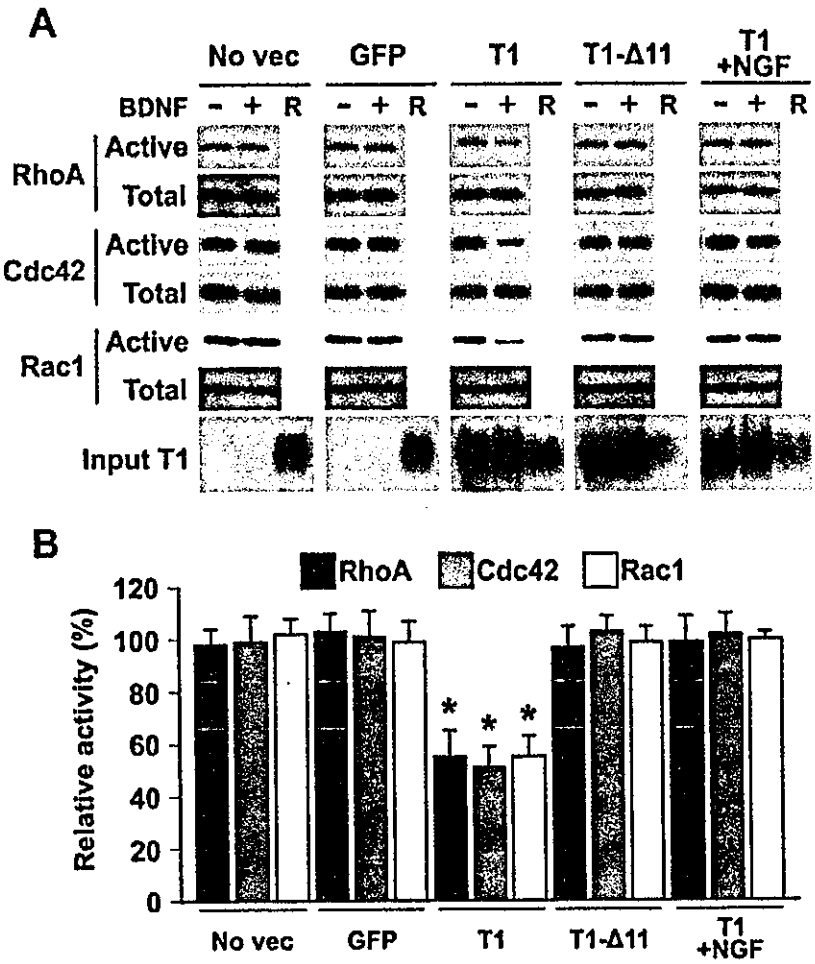

Figure 9. Activities of Rho GTPases in 2 DIV astrocytic cultures. *A*, No vec, No transfection; GFP, EGFP; T1, normal T1; T1-Δ11, a deletion form of T1 (see Fig. 1*C*); T1 + NGF, normal T1-expressing cells that were treated with 100 ng/ml NGF instead of BDNF. Cells were stimulated with vehicle (−) or with 20 ng/ml BDNF (+). The "R" in each column represents a rat brain sample. Overexpressed T1 and endogenous T1 from rat brain samples were detected by anti-T1 antibody, and overexpressed T1-Δ11 was detected by anti-pan-TrkB. Then, the precipitated proteins and total proteins (5 μg for RhoA; 100 μg for Cdc42 and Rac1) were loaded on 15% gel, and each protein was detected with a specific antibody. *B*, Quantitative analysis of Rho GTPase bands in *A*. Each control level, without BDNF stimulation, was taken as 100%. The asterisks indicate statistically significant differences ($p < 0.05$; paired Student's *t* test). Values are given as the means ± SD of four independent experiments.

References

Allendoerfer KL, Cabelli RJ, Escanòn E, Kaplan DR, Nikolics K, Shatz CJ (1994) Regulation of neurotrophin receptors during the maturation of the mammalian visual system. J Neurosci 14:1795–1811.

Aloyz R, Fawcett JP, Kaplan DR, Murphy RA, Miller FD (1999) Activity-dependent activation of TrkB neurotrophin receptors in the adult CNS. Learn Mem 6:216–231.

Araque A, Parpura V, Sanzgiri RP, Haydon PG (1999) Tripartite synapses: glia, the unacknowledged partner. Trends Neurosci 22:208–215.

Armanini MP, McMahon SB, Sutherland J, Shelton DL, Phillips HS (1995) Truncated and catalytic isoforms of trkB are co-expressed in neurons of rat and mouse CNS. Eur J Neurosci 7:1403–1409.

Barbacid M (1994) The Trk family of neurotrophin receptors. J Neurobiol 25:1386–1403.

Baxter GT, Radeke MJ, Kuo RC, Makrides V, Hinkle B, Hoang R, Medina-Selby A, Coit D, Valenzuela P, Feinstein SC (1997) Signal transduction mediated by the truncated trkB receptor isoforms, trkB.T1 and trkB.T2. J Neurosci 17:2683–2690.

Bibel M, Barde YA (2000) Neurotrophins: key regulators of cell fate and cell shapes in the vertebrate nervous system. Genes Dev 14:2919–2937.

Biffo S, Offenhäuser N, Carter BD, Barde YA (1995) Selective binding and internalization by truncated receptors restrict the availability of BDNF during development. Development 121:2461–2470.

Dechant G, Barde YA (1997) Signalling through the neurotrophin receptor $p75^{NTR}$. Curr Opin Neurobiol 7:413–418.

Eide FF, Vining ER, Eide BL, Zang K, Wang XY, Reichardt LF (1996) Naturally occurring truncated trkB receptors have dominant inhibitory effects on brain-derived neurotrophic factor signaling. J Neurosci 16:3123–3129.

Etienne-Manneville S, Hall A (2002) Rho GTPases in cell biology. Nature 420:629–635.

Fawcett JP, Bamji SX, Causing CG, Aloyz R, Ase AR, Reader TA, McLean JH, Miller FD (1998) Functional evidence that BDNF is an anterograde neuronal trophic factor in the CNS. J Neurosci 18:2808–2821.

Frisén J, Verge VM, Fried K, Risling M, Persson H, Trotter J, Hökfelt T, Lindholm D (1993) Characterization of glial trkB receptors: differential response to injury in the central and peripheral nervous systems. Proc Natl Acad Sci USA 90:4971–4975.

Fryer RH, Kaplan DR, Feinstein SC, Radeke MJ, Grayson DR, Kromer LF (1996) Developmental and mature expression of full-length and truncated TrkB receptors in the rat forebrain. J Comp Neurol 374:21–40.

Ghisdal P, Vandenberg G, Morel N (2003) Rho-dependent kinase is involved in agonist-activated calcium entry in rat arteries. J Physiol (Lond) 551:855–867.

Haapasalo A, Koponen E, Hoppe E, Wong G, Castrén E (2001) Truncated trkB.T1 is dominant negative inhibitor of trkB.TK+-mediated cell survival. Biochem Biophys Res Commun 280:1352–1358.

Hall A (1998) Rho GTPases and the actin cytoskeleton. Science 279:509–514.

Hartmann M, Heumann R, Lessmann V (2001) Synaptic secretion of BDNF after high-frequency stimulation of glutamatergic synapses. EMBO J 20:5887–5897.

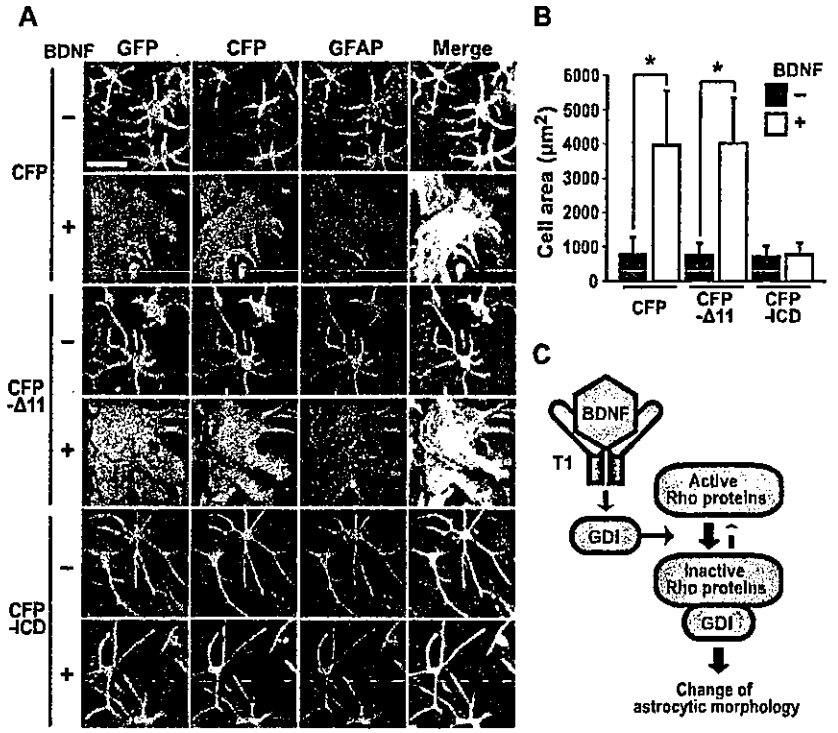

Figure 10. Competitive assay by overexpression of T1-specific C-terminal peptides. *A*, Expression vectors of T1 and CFP, CFP-Δ11, or CFP-ICD were cotransfected into astrocytes. CFP-Δ11 is a CFP-ICD lacking the 11 C-terminal amino acid residues. CFP-ICD is a fusion protein of CFP and the ICD segment of T1. The cells were stimulated with vehicle (−) or with 20 ng/ml BDNF (+). The cells with three overlapping colors are shown here in white. Scale bar, 50 μm. *B*, Quantification of each astrocytic area in *A*. Values are given as the means ± SD from the results of four independent experiments (total cell counts: CFP, without BDNF, $n = 859$, with BDNF, $n = 948$; CFP-Δ11, without BDNF, $n = 835$, with BDNF, $n = 960$; CFP-ICD, without BDNF, $n = 913$, with BDNF, $n = 955$). The asterisks indicate significant differences ($p < 0.05$; one-way ANOVA and Scheffé's *post hoc* test) from the values obtained without BDNF. *C*, Simplified schematic of the T1 signaling cascade. In astrocytes, the T1 signaling cascade acts as a negative inhibitor of the Rho GTPases in a BDNF-dependent manner, resulting in the morphological alteration of astrocytes. The bold lines indicate the signaling cascade promoted by BDNF. The broken lines indicate a lack of signal transduction.

Hirrlinger J, Hülsmann S, Kirchhoff F (2004) Astroglial processes show spontaneous motility at active synaptic terminals in situ. Eur J Neurosci 20:2235–2239.

Iino M, Goto K, Kakegawa W, Okado H, Sudo M, Ishiuchi S, Miwa A, Takayasu Y, Saito I, Tsuzuki K, Ozawa S (2001) Glia-synapse interaction through Ca^{2+}-permeable AMPA receptors in Bergmann glia. Science 292:926–929.

Illenberger D, Schwald F, Pimmer D, Binder W, Maier G, Dietrich A, Gierschik P (1998) Stimulation of phospholipase C-β_2 by the Rho GTPases Cdc42Hs and Rac1. EMBO J 17:6241–6249.

Just I, Selzer J, von Eichel-Streiber C, Aktories K (1995) The low molecular mass GTP-binding protein Rho is affected by toxin A from Clostridium difficile. J Clin Invest 95:1026–1031.

Kaplan DR, Miller FD (2000) Neurotrophin signal transduction in the nervous system. Curr Opin Neurobiol 10:381–391.

Klein R, Conway D, Parada LF, Barbacid M (1990) The *trkB* tyrosine kinase gene codes for a second neurogenic receptor that lacks the catalytic kinase domain. Cell 61:647–656.

Knüsel B, Rabin SJ, Hefti F, Kaplan DR (1994) Regulated neurotrophin receptor responsiveness during neuronal migration and early differentiation. J Neurosci 14:1542–1554.

Kohara K, Kitamura A, Morishima M, Tsumoto T (2001) Activity-dependent transfer of brain-derived neurotrophic factor to postsynaptic neurons. Science 291:2419–2423.

Kovalchuk Y, Holthoff K, Konnerth A (2004) Neurotrophin action on a rapid timescale. Curr Opin Neurobiol 14:558–563.

Kryl D, Barker PA (2000) TTIP is a novel protein that interacts with the truncated T1 TrkB neurotrophin receptor. Biochem Biophys Res Commun 279:925–930.

Maekawa M, Ishizaki T, Boku S, Watanabe N, Fujita A, Iwamatsu A, Obinata T, Ohashi K, Mizuno K, Narumiya S (1999) Signaling from Rho to the actin cytoskeleton through protein kinases ROCK and LIM-kinase. Science 285:895–898.

Mehta D, Ahmmed GU, Paria BC, Holinstat M, Voyno-Yasenetskaya T, Tiruppathi C, Minshall RD, Malik AB (2003) RhoA interaction with inositol 1,4,5-trisphosphate receptor and transient receptor potential channel-1 regulates Ca^{2+} entry. Role in signaling increased endothelial permeability. J Biol Chem 278:33492–33500.

Middlemas DS, Lindberg RA, Hunter T (1991) *trkB*, a neural receptor protein-tyrosine kinase: evidence for a full-length and two truncated receptors. Mol Cell Biol 11:143–153.

Offenhäuser N, Muzio V, Biffo S (2002) BDNF binding to truncated trkB.T1 does not affect gene expression. NeuroReport 13:1189–1193.

Ohira K, Hayashi M (2003) Expression of TrkB subtypes in the adult monkey cerebellar cortex. J Chem Neuroanat 25:175–183.

Ohira K, Shimizu K, Hayashi M (1999) Change of expression of full-length and truncated TrkBs in the developing monkey central nervous system. Brain Res Dev Brain Res 112:21–29.

Ohira K, Shimizu K, Hayashi M (2001) TrkB dimerization during development of the prefrontal cortex of the macaque. J Neurosci Res 65:463–469.

Oliet SHR, Piet R, Poulain DA (2001) Control of glutamate clearance and synapse efficacy by glial coverage of neurons. Science 292:923–926.

Ploug M, Jensen AL, Barkholt V (1989) Determination of amino acid compositions and NH_2-terminal sequences of peptides electroblotted onto PVDF membranes from tricine-SDS-PAGE: application to peptide mapping of human complement component C3. Anal Biochem 181:33–39.

Ren XD, Kiosses WB, Schwartz MA (1999) Regulation of the small GTP-binding protein Rho by cell adhesion and the cytoskeleton. EMBO J 18:578–585.

Ridley AJ (2001) Rho GTPases and cell migration. J Cell Sci 114:2713–2722.

Rose CR, Blum R, Pichler B, Lepier A, Kafitz KW, Konnerth A (2003) Truncated TrkB-T1 mediates neurotrophin-evoked calcium signalling in glia cells. Nature 426:74–78.

Sahara Y, Westbrook GL (1993) Modulation of calcium currents by a metabotropic glutamate receptor involves fast and slow kinetic components in cultured hippocampal neurons. J Neurosci 13:3041–3050.

Sasaki T, Takai Y (1998) The Rho small G protein family-Rho GDI system as a temporal and spatial determinant for cytoskeletal control. Biochem Biophys Res Commun 245:641–645.

Shelton DL, Sutherland J, Gripp J, Camerato T, Armanini MP, Phillips HS, Carroll K, Spencer SD, Levinson AD (1995) Human trks: molecular cloning, tissue distribution, and expression of extracellular domain immunoadhesins. J Neurosci 15:477–491.

Takai Y, Sasaki T, Matozaki T (2001) Small GTP-binding proteins. Physiol Rev 81:153–208.

Thoenen H (2000) Neurotrophins and activity-dependent plasticity. Prog Brain Res 128:183–191.

Yacoubian TA, Lo DC (2000) Truncated and full-length TrkB receptors regulate distinct modes of dendritic growth. Nat Neurosci 3:342–349.

Yamashita T, Tohyama M (2003) The p75 receptor acts as a displacement factor that releases Rho from Rho-GDI. Nat Neurosci 6:461–467.

Yamashita T, Tucker KL, Barde YA (1999) Neurotrophin binding to the p75 receptor modulates Rho activity and axonal outgrowth. Neuron 24:585–593.

Microbiol. Immunol., 48(12), 985–994, 2004

Editor-Communicated Paper

Quantum Dots Targeted to the Assigned Organelle in Living Cells

Akiyoshi Hoshino[1,2,3], Kouki Fujioka[1], Taisuke Oku[1,4], Shun Nakamura[5], Masakazu Suga[1], Yukio Yamaguchi[4], Kazuo Suzuki[3], Masato Yasuhara[2], and Kenji Yamamoto*[,1,2]

[1]*Department of Medical Ecology and Informatics, Research Institute, International Medical Center of Japan, Shinjuku-ku, Tokyo 162–8655, Japan,* [2]*Department of Pharmacokinetics and Pharmacodynamics, Hospital Pharmacy, Tokyo Medical and Dental University, Bunkyo-ku, Tokyo 113–8519, Japan,* [3]*Department of Bioactive Molecules, National Institute of Infectious Diseases, Shinjuku-ku, Tokyo 162–8640, Japan,* [4]*Department of Chemical System Engineering, School of Engineering, University of Tokyo, Bunkyo-ku, Tokyo 113–8656, Japan, and* [5]*Division of Biochemistry and Cellular Biology, National Institute of Neuroscience, Kodaira, Tokyo 187–8502, Japan*

Communicated by Dr. Hidechika Okada: Received October 8, 2004. Accepted October 21, 2004

Abstract: **Fluorescent nanocrystal quantum dots (QDs) have the potential to be applied to bioimaging since QDs emit higher and far longer fluorescence than conventional organic probes. Here we show that QDs conjugated with signal peptide obey the order to transport the assigned organelle in living cells. We designed the supermolecule of luminescent QDs conjugated with nuclear- and mitochondria-targeting ligands. When QDs with nuclear-localizing signal peptides were added to the culture media, we can visualize the movements of the QDs being delivered into the nuclear compartment of the cells with 15 min incubation. In addition, mitochondrial signal peptide can also transport QDs to the mitochondria in living cells. In conclusion, these techniques have the possibility that QDs can reveal the transduction of proteins and peptides into specific subcellular compartments as a powerful tool for studying intracellular analysis *in vitro* and even *in vivo*.**

Key words: **Quantum dot, Signal peptide, Nanocrystal, Nuclear localizing signal, Mitochondria targeting signal, Bioimaging**

Nanotechnology is the technology of designing, manufacturing, and utilizing the "supermolecule materials" which have the specific function based on their nanometer size. The "supermolecule" said here is a functional unit of two meanings; (1) A supermolecule consists of each molecule that has a certain mutual interaction and relation with one another, (2) A supermolecule shows its specific function as a whole molecule. Ultrafine nanocrystals have been expected to be applied widely in biomedical fields as biomaterials, immunoassay, diagnostics, and even in therapeutics (7, 9, 18, 32, 34, 40, 41). One of them, nanocrystal quantum dots (QDs), is widely used as stable and bright fluorophores that can have high quantum yields, narrow luminescent spectra, high absorbency, high resistance to photobleaching, and can provide excitation of several different emission colors using a single wavelength for excitation (4, 19).

In the field of molecular biology, fluorescent tagging of cells and biomolecules with organic fluorophores such as FITC has been used for a long time for these purposes of tracking biomolecules. But unfortunately, the use of organic fluorophores for living-cell applications is subject to certain limitations, because most of fluorophores photobleach easily (17). These organic fluorophores have their broad emission bands, which limit the number of fluorescent probes that can be simultaneously resolved. In addition, there are a lot of bright fluorophores, such as Hoechst® dyes and a rhodamine 123 derivative (Mitotracker®) (20), used for stain of nuclei and mitochondria, but these fluorophores cannot transport proteins or other molecules to the target

Address correspondence to Dr. Kenji Yamamoto, Department of Medical Ecology and Informatics, Research Institute, International Medical Center of Japan, Toyama 1–21–1, Shinjuku-ku, Tokyo 162–8655, Japan. Fax: +81–3–3202–7364. E-mail: backen@ri.imcj.go.jp

Abbreviations: MPA, 3-mercaptopropanoic acid; QD, quantum dot; TOPO, *n*-trioctylphosphine oxide.

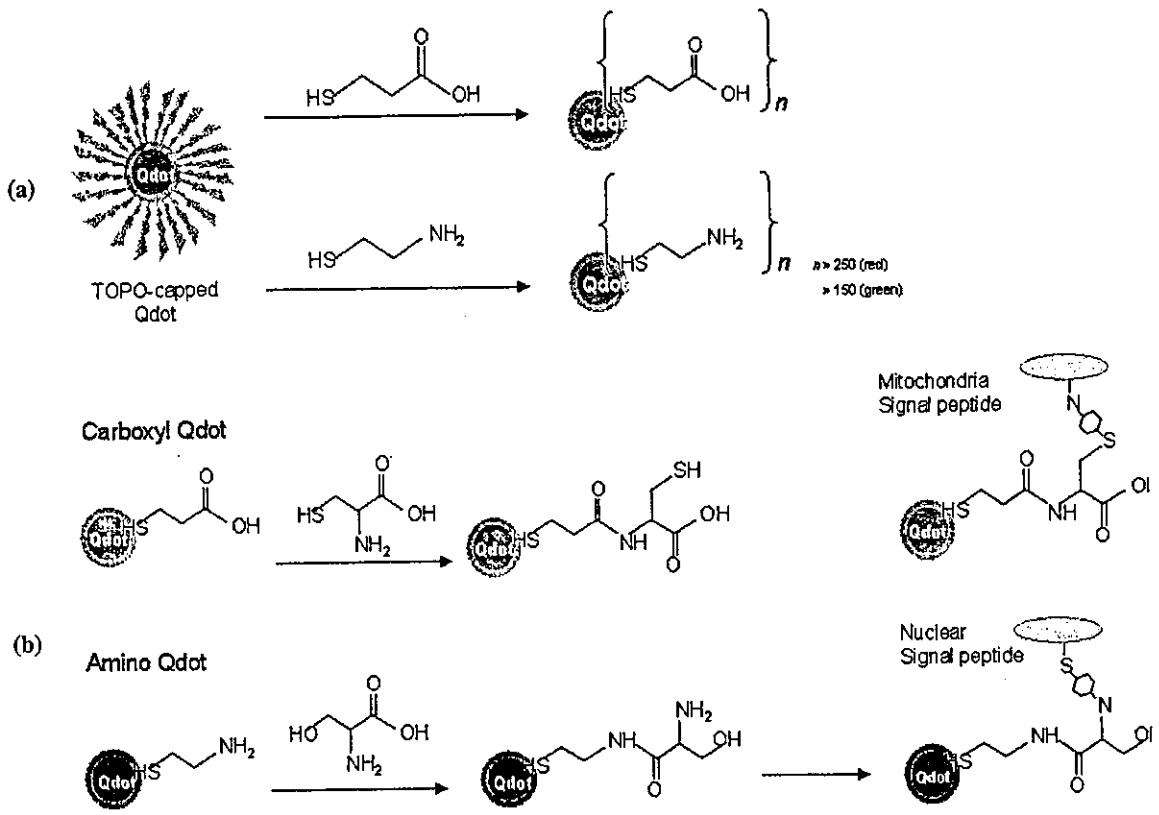

Fig. 1. Schematic illustration of peptide conjugated QDs for organelle targeting and imaging. (a) Chemically synthesized TOPO-capped QDs were replaced by MPA or cysteamine using thiol-exchange reactions. After reaction, QDs were covered with approximately 250 carboxyl or amine groups per particle. (b) A two-step conjugation strategy of QD-oligopeptide probes. MPA-QD (upper lane) or cysteamine-QD (lower lane) was primarily coupled with amine groups of cysteine or serine by using EDC coupling reagents. Then amino acid-coated QDs were secondarily conjugated with target peptides by coupling between *N*-hydroxysuccinimidyl and maleimide groups.

organelle. On the other hand, the signal peptides with organic fluorophore cannot trace the luminescent for long time observation. In contrast, QDs are stabilized over a far longer exposure-time to light and can emit fluorescence of higher luminosity than the conventional organic fluorescence probes (5, 8, 27). Therefore, QDs are suitable for designing the supermolecule that supplemented the biological effects to itself, and applications with QDs are now widely performed as long-time fluorescent markers for efficient collection of fluorescence (3, 17, 22, 24, 35).

Once our synthesized QDs were enfolded into the hydrophobic micelles and completely dissolved in aqueous solution, which promotes several innovations to improve the solubility to apply for biological methods (2, 10, 11, 23). The water-soluble QDs in our previous method have lower stability for low pH or salt-containing buffer (14). There is very little amount of conjugate by using these QDs, since the most of QDs were easily aggregated under the conditions that combine QD with peptides or protein. Therefore, we could only utilize QDs as the high fluorescence cell-tracking markers (14, 33). We previously reported that several novel surface-modified QDs using carboxylic acids, polyalcohols, or amines showed various physicochemical properties (16). In this article, we established a two-step conjugating method as shown in Fig. 1. The QDs of carboxyl groups were primarily coupled with amine groups of cysteine monomer, and QDs of amine groups were with carboxylic groups of serine monomer, respectively. The obtained amino acid-coated QDs, which were stable for the pH changes, were secondarily conjugated with target peptides/proteins by using their sulfhydryl and amine groups.

Some proteins and peptides have been demonstrated to penetrate through the plasma membrane of cells by their protein transduction domains (12, 21, 26, 31). Previous studies defined that protein transduction by nuclear localizing peptides was an efficient method to deliver proteins into the nuclei of cells (25, 37). In this study we tried to label two functional oligopeptides transported to nuclear localizing or mitochondria, and

evaluated whether QD-peptide complex worked as the specific functional supermolecule based on original peptides.

Materials and Methods

Synthesis of hydrophilic QDs. Synthesis of ZnS-coated CdSe nanocrystal QDs (fluorescence wavelength: approximately 642 nm emitted red, and approximately 518 nm emitted green), which were enfolded into the micelle of *n*-trioctylphosphine oxide (TOPO), was previously reported (6, 15). 3-Mercaptopropanoic acid (MPA) and 2-aminoethanethiol (cysteamine hydrochloride) were used to obtain two kinds of hydrophilic QDs (carboxyl- and amino-QDs) by thiol exchange methods. In the case of carboxyl-QD, 50 mg of TOPO-QDs were dissolved into 1 ml tetrahydrofuran (THF) in a 4 ml-volume flasket, and then 250 μl MPA (Sigma-Aldrich, St. Louis, Mo., U.S.A.) were added. Then the mixture was heated at 85 C for 24 hr. In the case of amino-QD, primarily 250 mg cysteamine (Wako Pure Chemicals, Tokyo) was heated at 85 C in a flask (16). After melting, 50 mg/ml TOPO-QDs in THF was dropped to the flask and heated at 85 C for 2 hr. After the reaction, the turbid solution was collected and centrifuged at maximum speed. After it dried up, purified water was added to the residue, and centrifuged at maximum speed to remove the insoluble residue. The supernatant fraction containing soluble QDs was collected. After purified by Sephadex G-25 column (Amersham Biosciences, Piscataway, N.J., U.S.A.), QDs were concentrated and powderized by vacuum distillation. QDs were reconstituted in purified water before use.

Preparation of peptide-conjugated QDs. Amino acid sequences of three well-known functional oligopeptides described below were chemically synthesized; nuclear localizing peptide ($R_{11}KC$, sequenced NH_2-RRRRRRRRRRKC-COOH) (25), mitochondria targeting signal sequence of cytochrome-*c* oxidase VIII subunit (Mito-8, sequenced NH_2-MSVLTPLLLRGLTGSARRLPVPRAKIHWLC-COOH) (13) or control mitochondrial peptide (START, sequenced NH_2-STARTSTARTSTARTSC-COOH) (1). The peptides were conjugated to QDs by a two-step reaction. Initially, 100 μM QD solution was mixed with equal volume of 100 mM cysteine solution in coexistent with 100 mM EDC coupling reagents (Pierce Biotechnology, Rockford, Ill., U.S.A.) and continuously mixed at 4 C for 1 hr. After removed of free-amino acid by Nap-5 column (Amersham Biosciences), about 10-fold mol of target peptides were secondarily conjugated with QD by using sulfo-SMCC coupling reagents (Pierce Biotech) and sonicated for 2 hr at 4 C. Products were purified using ultra-filtration membrane (NMWL 10000, Centriprep® Millipore). Finally, purified QD-peptide conjugates were filtrated with 0.1-μm membrane filters (Millipore) before use. To analyze the protein content of QD-conjugated peptides, conjugated QDs was plated to 96-well microplate and RC-DC Protein Assay reagent (Bio-Rad, Hercules, Calif., U.S.A.) was added. Six hundred fifty nanometer absorbance was measured by microplate reader (Bio-Rad). MPA-coated QD without coupling with any peptides was used as negative control.

Assessment of QD-uptake by cells. Vero cells were cultured in DMEM/F12 supplemented with 5% heat-inactivated fetal bovine serum at 37 C. To avoid the non-specific binding of QDs on the glass, 10 mm glass-based culture dish (Matsunami Glass Industries, Japan) was pre-coated with poly-L-lysine (Peptide Institute Co., Ltd., Osaka, Japan). The cells were plated at a volume of 1×10^5 cells/well on a glass-based dish. Then cells were stimulated with the indicated concentration of QD-peptides. After incubation, the cells were washed with PBS 5 times to remove the non-specific binding QDs, and the cells were fixed, and embedded in the glycerol containing 0.1% sodium azide. In the case of co-localization assay, cells were observed with a confocal microscopy MRC-1024 (Bio-Rad). Time course of $R_{11}KC$-coated QDs was examined on the fluorescence microscopy system equipped with a CO_2 incubator (IM-310 cell-culture microscope system, Olympus, Japan). Images were acquired with a digital camera D1X (Nikon) under fluorescent microscopy IX-81 (Olympus) using WIR mirror unit to adjust excitation wavelength over 610 nm.

Results and Discussion

Some oligopeptides have been demonstrated to penetrate across the cellular membrane by their protein transduction domains and specifically located to their designated organelle (12, 21, 26, 31). Previous studies showed that the protein transduction by nuclear localizing signal oligopeptide was an efficient method of delivering proteins into the nuclei of cells (37). To establish the supermolecule design that supplemented the biological effects to nanocrystal, we conjugated two kinds of functional NLS and MTS oligopeptides, which were transported to nuclear or mitochondria (13, 25). Then we evaluated that QD-peptide complex worked as the specific supermolecule those functions were based on their original peptides.

For the achievements of assemble QD-supermolecule, we established a two-step conjugating method as shown in Fig. 1. Briefly, QDs were coupled with amino

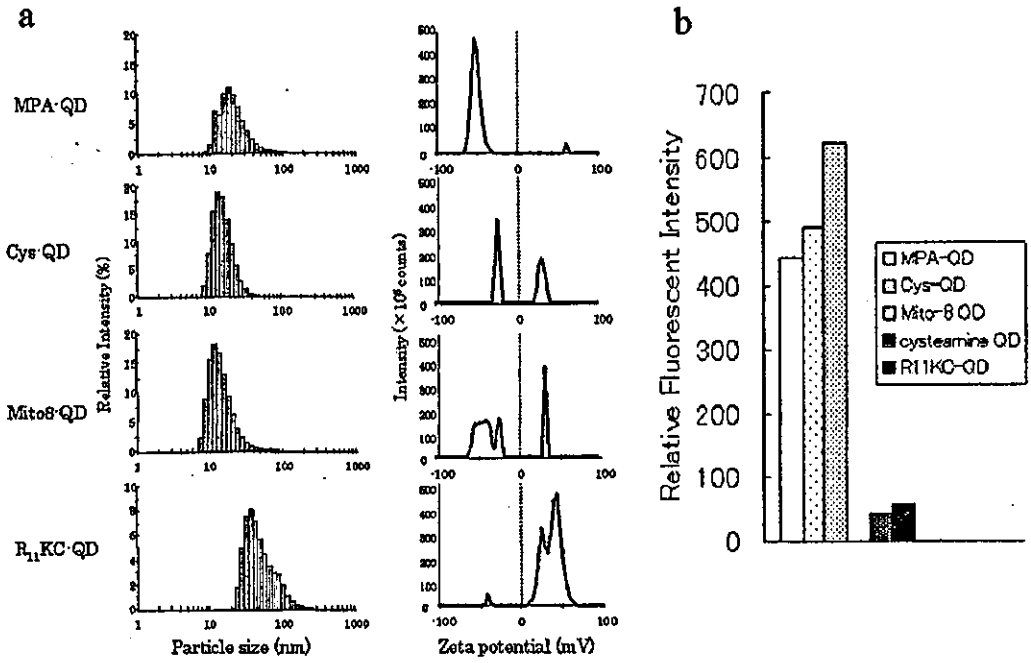

Fig. 2. Physicochemical properties of oligopeptide-conjugated QDs. (a) Particle size distribution of various QDs in aqueous solution (left) was measured by dynamic light scattering methods. Values are the mean±standard deviation of the data measured 12 times, respectively. Surface ζ-potential of QDs (right) was measured by electrophoresis. The line shows the electrophoretic mobility of these QDs in the stationary layers of 30 assays. Data shows the average of 30 assays. (b) Relative fluorescence intensity of QDs solution (10 μM) were measured by fluorospectrometer. QDs were excited by 365 nm wavelength (UV-A) and luminescence intensity of peak emission wavelength (519 nm) was detected.

acid at the first step, and secondarily coupled with the target oligopeptide. We prepare two kinds of QD whose surfaces were covered with carboxyl and sulfhydryl, and with NH_2 and hydroxyl groups, respectively. MPA-QDs were primarily coupled with amine groups of cysteine by using EDC coupling reagents (cys-QD). In the case of amine-QDs, they were also coupled with carboxylic groups of serine (ser-QD). The surface of the obtained QD was covered with approximately 450 amino acids per particle (data not shown). Both of the newly obtained amino acid-coated QDs, which were stable for changes of pH, were secondarily conjugated with target peptides by coupling with their sulfhydryl and amine groups by sulfo-SMCC reagents. In this study, we conjugated two kinds of signaling peptide; nuclear localizing signal (NLS) oligopeptide $R_{11}KC$ (25), and mitochondria targeting signal (MTS) oligopeptide Mito-8 (13). Mito-8 peptides were coupled with cys-QDs, and basic $R_{11}KC$-peptides were with ser-QDs, respectively. The number of peptide with QDs were calculated based on RC-DC protein assay, indicating that QD-$R_{11}KC$ and QD-Mito-8 were covered with 48 and 62 peptides per particle, respectively (data not shown). To assess the change of physicochemical properties of QDs after conjugated with oligopeptides, the particle size and surface potential of peptide-conjugated QDs were observed by a dynamic light scattering method. This surface potential of QDs was drastically changed after conjugated with peptides (Fig. 2a). In this labeling method, the average of the observed particle size distribution tends to increase, because it is hardly avoidable to control the excess polymerization. Previously, we tried to target signal peptides directly to MPA-QDs, resulted in aggregation, especially in the case of amine-rich oligopeptides because of salt-formation between carboxylic groups of QD and amine groups of target peptides (16). This novel two-step method enables to QDs labeled even in amine-rich basic oligopeptides such as $R_{11}KC$. Our previous study demonstrated that the fluorescence intensity of QD was also dramatically changed by the surface-covered molecules of QD particle (16, 22). We previously tried to cover QDs directly with cysteine monomer, which resulted in losing luminescence during the labeling process, because of electron leakage through the surface NH_2 group (16). Therefore, we assessed whether the fluorescent intensity of QDs changed or diminished during the peptide coupling process. After the first reaction step, slight change of luminescent intensity was observed. But the fluores-

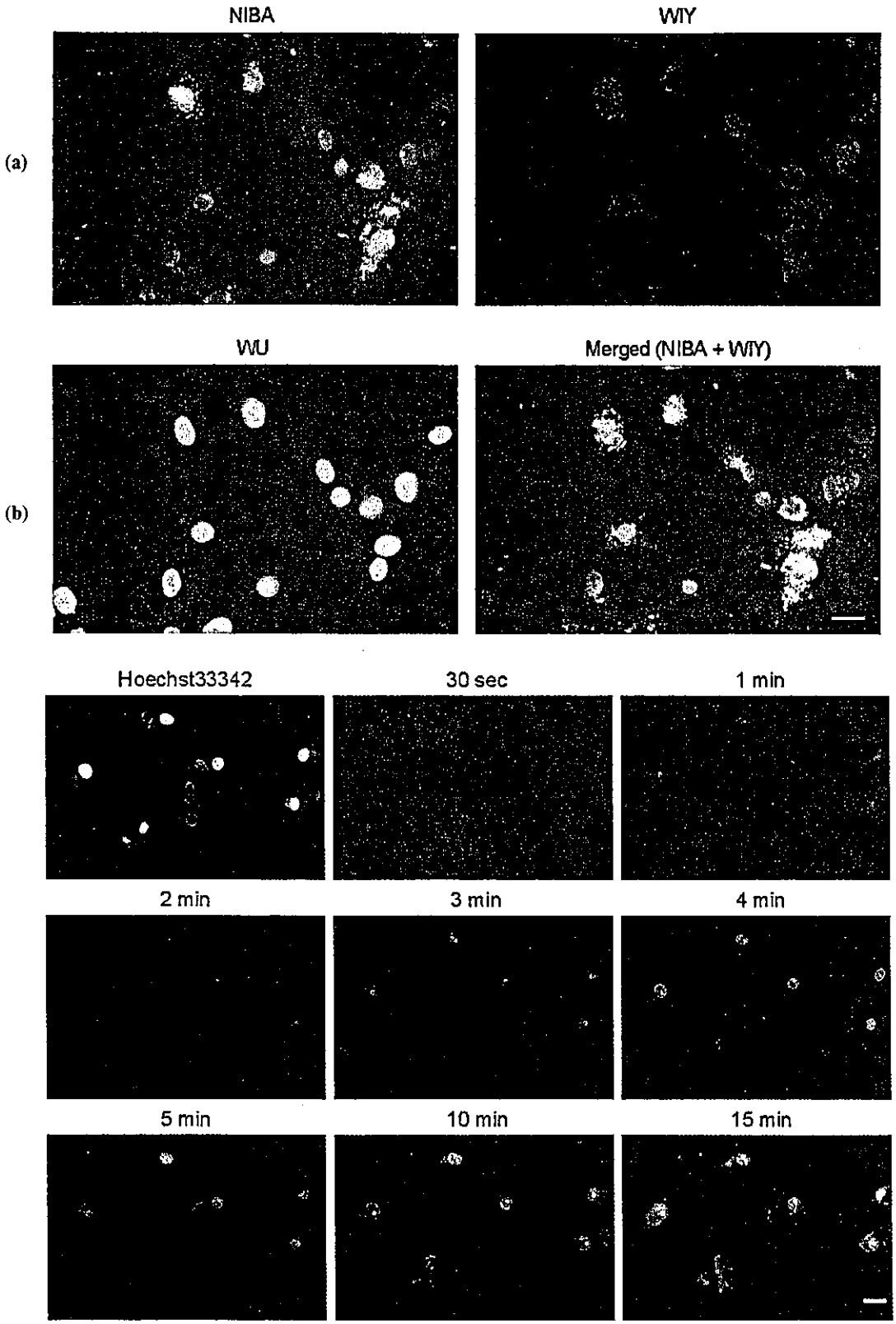

Fig. 3. Localization of $R_{11}KC$-conjugated QDs to nucleus. (a) Cells were pre-stained with Hoechst®33342, and stimulated with FITC-labeled QD-conjugated $R_{11}KC$ peptide (1 μM final) for 3 hr at 37 C with 5% CO_2 condition. (b) Cells were pre-stained with Hoechst®33342, and stimulated with QD-$R^{11}KC$ (1 μM final) for the indicated time at 37 C under 5% CO_2 condition with a culture fluorescence microscope (IM-310 system, Olympus). Images were taken using D1X digital camera (Nikon) equipped with IM-310 system at the indicated time by a 3 sec exposure. Bars indicated 10 μm.